Aus dem Centrum für Schlaganfallforschung (CSB)
der Medizinischen Fakultät Charité – Universitätsmedizin Berlin

DISSERTATION

How short can we go?
The impact of BOLD delay scan length on detecting hypoperfusion.

Wie kurz darf es sein?
Der Einfluss der BOLD Delay Scan Länge auf die Erkennung von Hypoperfusionen.

zur Erlangung des akademischen Grades
Doctor medicinae (Dr. med.)

vorgelegt der Medizinischen Fakultät
Charité – Universitätsmedizin Berlin

von

AYSE CEREN TANRITANIR

aus Bursa, Türkei

Datum der Promotion: 23 März 2024

Inhaltsverzeichnis

Abbildungsverzeichnis:

Abkürzungen:

BOLD: Blood Oxygen Level Dependent

fMRI: Functional Magnetic Resonance Imaging

NIRS: Near-infrared Spectroscopy

sLFOs: systemic Low Frequency Oscillations

DSC-MRI: Dynamic Susceptibility Contrast Magnetic Resonance imaging

DWI: Diffusion-weighted Imaging

FD: Framewise Displacement

DSC: Dice Similarity Coefficient

PCC: Pearson Correlation Coefficient

KW: weighted Cohen's Kappa

LoA: Limits of Agreement

CI: Confidence Interval

MTT: Mean Transit Time

ASL: Arterial Spin Labelling

EPI: Echo-planar Imaging

TR: Repetition Time

TE: Echo Time

TIA: Transient Ischemic Attack

RIPTiDe: Regressor Interpolation at Progressive Time Delays

AFNI: Analysis of Functional Neuroimages

FSL: FMRIB (functional magnetic resonance imaging of the brain) Software Library

FOV: Field Of View

ANTs: Advanced Normalization Tools

IQR: Interquartile Range

OR: Odds Ratio

Zusammenfassung

Einleitung:

Die nicht-invasive Erkennung von Hypoperfusionen mithilfe der "BOLD *(„blood-oxygenation-level-dependent“)* Delay" ist eine relativ neue Methode. Frühere BOLD Delay Studien verwendeten längere Scans als für etablierte Perfusionsbildgebungsmethoden üblich. Der Effekt der Verkürzung dieser Scans ist noch nicht bekannt. Hier haben wir systematisch den Einfluss der Scanlänge auf die Beurteilung der Hirnperfusion mit BOLD delay bewertet.

Methode:

63 Patienten mit akutem Schlaganfall unterzogen sich einem Standardprotokoll für die Schlaganfall Bildgebung, einschließlich eines Multiband EPI Scans for BOLD Delay Mapping (CMRR, TR / TE = 400/30 ms, Flipwinkel 43 °, Multiband-Faktor = 6, dreißig 4,0-mm-Schnitte, Erfassungszeit : 340s). Um eine repräsentative klinische Population zu spiegeln, wurden Patienten aufgrund von Kopfbewegungen nicht ausgeschlossen. Eine Untergruppe von 43 Patienten mit sichtbarer Hypoperfusion auf BOLD Delay Maps wurde für die quantitative Analyse ausgewählt.

Die Resting-state Daten (rsfMRI) von 63 Patienten mit akutem ischämischen Schlaganfall wurden in 5 progressiv verkürzte Scan Segmente unterteilt. Die Qualität und der diagnostische Nutzen der von jedem Segment erzeugten BOLD Delay Maps wurden von zwei Radiologen bewertet. Für den qualitativen Vergleich kürzerer Scans mit dem durchgehenden Scan Segment wurden binäre logistische und ordinale gemischte Modelle durchgeführt. Wir analysierten auch den Effekt der Scanlänge auf das Volumen der Hypoperfusion Läsionen unter Verwendung des Bland-Altman-Diagramms und lineare gemischte Modelle für die quantitative volumetrische Analyse der Untergruppe. Kopfbewegungen wurden in den gemischten Modellen immer berücksichtigt.

Ergebnisse:

Logistische und ordinale gemischte Modelle zeigten, dass eine Verkürzung der Scanlänge um 60% die Qualität der BOLD Delay Maps (OR 0,3 [0,2, 0,46]) und ihre Sensitivität für die Erkennung von Hypoperfusionen (OR 0,33 [0,18, 0,59]) drastisch verringerte. Lineare gemischte Modelle zeigten jedoch, dass verschiedene Scan Segmente nicht systematisch mit der volumetrischen Schätzung von Hypoperfusion Läsionen assoziiert waren. Kopfbewegung beeinträchtigt Struktur Klarheit und vermehrt Bildrauschen.

Diskussion:

Diese Studie untersuchte systematisch den Effekt der Reduzierung der Scanzeit auf die diagnostische Qualität der BOLD Delay Maps bei akutem Schlaganfall. Zur Beurteilung der Perfusion mithilfe der BOLD Delay kann die Scanzeit auf 3 Minuten und 24 Sekunden reduziert werden, ohne dass die Diagnosestellung und die Bildqualität wesentlich beeinträchtigt werden. Die Schätzungen des Volumens der Hypoperfusion Läsionen waren bis zu einer Scanzeit von 1 Minute und 8 Sekunden robust. Unsere Ergebnisse sind ein wichtiger Schritt in Richtung Kontrastmittel-freie BOLD Delay Technik zur Erkennung von Hypoperfusionen.

Abstract

Background:

Noninvasively detecting hypoperfusion using blood oxygen level dependent (BOLD) delay is a relatively new method. Previous BOLD delay studies used longer scans than typical of established perfusion imaging methods. The effect of shortening these scans is not yet known. Here, we systematically evaluated the impact of scan length on brain perfusion assessment with BOLD delay.

Method:

Sixty-three acute stroke patients underwent a standard stroke imaging protocol including multiband EPI scans for BOLD delay mapping (CMRR, TR/TE=400/30 ms, flip angle 43°, multiband factor=6, thirty 4.0-mm slices, acquisition time: 340s). To reflect a representative clinical population, patients were not excluded based on head motion. A subset of 43 patients with visible hypoperfusion on BOLD delay maps were selected for quantitative analysis.

Resting state functional MRI (rsfMRI) data of 63 patients with acute ischemic stroke were divided into 5 progressively shortened scan segments. The quality and diagnostic utility of the BOLD delay maps generated by each segment were assessed by two readers. Binary logistic and ordinal mixed effects models were executed for the qualitative comparison of shorter scans with the full-length scan. We also analyzed the effect of scan length on the hypoperfusion lesion volumes using Bland-Altman plot and linear mixed effects models for the quantitative volumetric analysis of the subset group. Head motion was always accounted for in the mixed effects models.

Results:

Binary logistic and ordinal mixed effects models showed that shortening the scan length by 60% diminished the quality of the maps (OR 0.3 [0.2, 0.46]) and their sensitivity to hypoperfusion detection (OR 0.33 [0.18, 0.59]) drastically. However, linear mixed effects models revealed that various scan segments were not systematically associated with volumetric estimation of lesions. Head motion adversely altered noise and structure clarity on the BOLD delay maps.

Discussion:

This study methodically assessed the effect of scan time reduction on the diagnostic quality of BOLD delay perfusion mapping in acute stroke. For assessment of perfusion using BOLD delay, scan time can be reduced to 3 min 24 sec without a significant loss of diagnostic accuracy and image quality. Hypoperfusion lesion volume estimates were robust down to 1 min 8 sec scan time. Our results provide an important step towards the implementation of contrast agent-free BOLD delay mapping for detecting hypoperfusion.

Background:

Definition of stroke:

The current World Health Organization definition of stroke (introduced in 1970 and still used) is “rapidly developing clinical signs of focal (or global) disturbance of cerebral function, lasting more than 24 hours or leading to death, with no apparent cause other than that of vascular origin (1).
Another updated definition has also been made recently: “Stroke is classically characterized as a neurological deficit attributed to an acute focal injury of the central nervous system (CNS) by a vascular cause, including cerebral infarction, intracerebral hemorrhage (ICH), and subarachnoid hemorrhage (SAH), and is a major cause of disability and death worldwide (2).

Epidemiology:

In 2019, ischaemic heart disease and stroke were the top-ranked causes of disability-adjusted life-years (DALYs) in both the 50–74-year and 75-years-and-older age groups (3).

Stroke is worldwide and in Germany the second leading cause of death and one of the most common causes of disability in adulthood (Robert Koch-Institut (Hrsg.) (2015) Kapitel 2.3.2: Schlaganfall. In: Gesundheit in Deutschland. Gesundheitsberichterstattung des Bundes. Gemeinsam getragen von RKI und Destatis. RKI, Berlin, S. 43–50) (4).

The 12-month prevalence of a stroke or chronic complaints as a result of a stroke in people under 55 years have been shown to be less than 1%. After that, it rises disproportionately to 6.4% for women and 6.1% for men aged 75 and over (12-Monats-Prävalenz von Schlaganfall oder chronischen Beschwerden infolge eines Schlaganfalls in Deutschland rki).

As noted earlier, the risk of stroke increases with age and doubles over the age of 55 years in both men and women (5). Although it has been known that one of

the most predisposing factors to stroke is an older age, stroke may occur at younger ages too.

Pathophysiology:

Stroke is caused by deficient blood and oxygen supply to the brain. In ischemic stroke the cause of that deficient supply is a blocked vessel. Hemorrhagic stroke, however, is because of bleeding or leaky blood vessels (5).

Ischemic stroke:

Ischemic occlusions contribute to around 85% of casualties of stroke cases. Ischemic occlusion is generated by thrombotic and embolic conditions in the brain. In an embolic stroke, the blood flow to the brain region decreases following an embolism; the blood flow to the brain reduces, causing severe stress and ultimately cell death (necrosis) (5). Necrosis is followed by disruption of the plasma membrane, organelle swelling and leaking of cellular contents into extracellular space (6), and loss of neuronal function.

Hemorrhagic stroke:

Hemorrhagic stroke accounts for approximately 10–15% of all strokes and has a high mortality rate. In 2015, about 3.0 million deaths resulted from ischemic stroke while 3.3 million deaths resulted from hemorrhagic stroke (7). In this condition, stress in the brain tissue and internal injury cause blood vessels to rupture. It produces toxic effects in the vascular system, resulting in infarction (8). It is classified into intraparenchymal and subarachnoid hemorrhage.

Complications:

Stroke may result in countless complications where detection of the early signs of it becomes crucial (9).

One of the most severe complications is cerebral edema (CED). It is the cause of death in 5% of all patients with cerebral infarct (10). The formation of cerebral edema includes three stages (cytotoxic edema, ionic edema, and vasogenic edema) (11) . Vasogenic edema is extracellular accumulation of water. It arises from an increased permeability of the blood-brain barrier and in this context by the passage of plasma from the vessels into the interstitium (12). Both forms of edema lead to an increase in intracerebral pressure, which can lead to pressure-related complications, such as herniations.

Imaging as diagnosis of stroke:

There are multiple ways for detecting stroke, but CT, especially non-contrast, and MRI are the most commonly used methodologies in emergency medicine.

Studies suggest that non-contrast CT is insufficiently sensitive for the diagnosis of acute ischaemia, is subject to substantial inter-rater variability in interpretation, and might not be better than MRI for detection of acute intracranial haemorrhage. (13) (14).

MRI offers advantages for the assessment of acute stroke. Changes of acute ischaemic injury are detectable sooner with MRI, especially with diffusion-weighted imaging, and ischaemic stroke diagnosis with MRI has greater interobserver and intraobserver reliability, even in readers with little experience. (15) (16).

It has been also shown that MRI has a higher sensitivity than CT for all acute strokes and for acute ischaemic stroke (17).

Hypoperfused area and detection of penumbra:

Following the occlusion of a brain artery, the blood flow is reduced in that local area. However, there is an area called the ischemic penumbra which is characterized by severely reduced blood flow where salvation of the normal electrical neural activity is still possible (18). The penumbra represents the tissue at risk of being permanently damaged as time passes. Its detection allows treatment of patients who would otherwise be excluded, such as those presenting beyond conventional time windows or without detectable infarction at presentation (19) (20).

The detection of the penumbra allows us to assess the perfusion-diffusion mismatch which is a widely-used measure while deciding for an appropriate treatment during an ischemic condition in an acute clinical setting (21). There are multiple approaches that can be used to visualize the penumbra in clinical practice . Dynamic susceptibility contrast MRI (DSC-MRI) is used most commonly, where a paramagnetic contrast agent (usually gadolinium-based) is injected intravenously. However, this technique has its limitations, e.g. potential side effects of gadolinium. These include kidney damage (22) and long-term deposition in the brain (23), the consequences of these are yet to be understood fully.

Another commonly used method that does not require an exogenous contrast agent is arterial spin labeling (ASL). But it has certain drawbacks compared to DSC-MRI, including low SNR and an innate sensitivity to head motion (24). These make it difficult to interpret the results in patients with severe atherosclerotic disease affecting the large vessels when the time it takes the labeled blood to travel from the labeling area to the measurement area is unknown (25). Drawbacks of existing methods have motivated a search for new

techniques for perfusion measurement in brain which could be applicable in clinical practice such as the use of blood-oxygenation-level-dependent (BOLD) signal as an endogenous source of blood flow contrast where intravenous contrast agent is not needed (26).

Bold delay method as perfusion measurement technique in brain:

The effect of deoxyhemoglobin on R2* is the basis of the BOLD signal. BOLD signal fluctuations occurring in low frequencies (between 0.01 and ~0.1 Hz) represent non-neural signals that can also be measured using NIRS (near-infrared spectroscopy) (27).

The non-neuronal low frequency oscillations, referred to as systemic low-frequency oscillations (sLFOs) (27–32), reflect the passage of cerebral blood via their propagation from the periphery to and through the brain (27). Therefore, sLFOs have been shown to provide similar information about local blood flow disturbances to DSC-MRI in diseases such as ischemic stroke (20) (33) (26,34–36), transient ischemic attack (TIA) (37), Moyamoya disease (38) and patients with other chronic cerebrovascular diseases such as carotid occlusion (39). These local blood flow disturbances are reflected as the delay in the arrival of sLFOs to a certain voxel relative to their arrival in a reference region, defined as BOLD delay.

Research goals and objectives:

The clinical applicability of BOLD delay is still limited due to its long acquisition time. Studies utilizing BOLD delay for brain perfusion assessment varied widely in scan duration, between 3.36 and 30 minutes (20) (33) (26) (34–36) (38) (40) (31,41). These studies had longer acquisition times than those typical of DSC-MRI (~2 min).

This variability could be because a systematic evaluation of the effect of scan length on BOLD delay mapping is lacking, thus a consensus on optimal scan duration for detecting hypoperfusion under various clinical circumstances (e.g. acute and chronic stroke) has not yet been reached.

This study focuses on evaluating the impact of scan length on various features of BOLD delay maps generated using the BOLD delay method for assessing brain perfusion in acute stroke patients. These features were the lesion volume estimation, diagnostic accuracy and image quality.

This study should also be regarded as a revalidation of a relatively new technique called Time Shift Analysis for systematically analyzing above mentioned low-frequency oscillations. With the help of the Time Shift Analysis, we were able to track the arrival of these oscillations to a certain voxel in comparison to the reference region if there is a blood flow disturbance. This helped us generate BOLD delay maps. The details of the Time Shift Analysis is explained below in the Methods section.

Our study used multiband echo planar imaging which has never been applied in other BOLD delay studies assessing brain perfusion. It pushes the temporal resolution of MRI high enough for the assessment of local hemodynamic response of sLFOs while removing the aliasing signals from the high frequency range as much as possible. The importance of using a higher TR in order to eliminate aliasing signals more effectively is explained in more detail in the following chapters.

Furthermore, we were able to assess the interrater agreement of this brand new method for brain perfusion measurement. We asked two expert neuroradiologists to evaluate plenty of BOLD delay maps and judge their interpretability and other various qualitative features of the maps. We compared the interrater agreement of the BOLD delay method with ASL (arterial spin labeling) which is used for

brain perfusion assessment and does not require intravenous contrast injection as well.

Method:

Systemic low-frequency-oscillations and the Time-Shift Analysis:

A substantial part of the measured BOLD signal is generally below 0.15 Hz (42), since it represents a convolution of fast synaptic activity with the local slow hemodynamic changes occuring in response to that activity (43). However, neuronal signals are not the only contributors to BOLD signals at this low frequency band, and sLFOs are regarded as one of those non-neuronal fluctuations in brain hemodynamics. They are unavoidable, spontaneous, physiological oscillations, propagate with the blood and have an extracerebral origin, accounting for 20 to 70% variance in the BOLD signal itself (44). Fast respiratory and cardiac fluctuations are known to alias in sLFOs and may contribute to this variance (28,30–32,45), along with variations in heart-rate and respiratory volume (46) . They oscillate at the same frequencies as neuronal and local vascular LFOs and cause changes in R2* that are similar to those caused by neurovascular coupling, unlike the much faster BOLD signal changes caused by cyclical cardiac and respiratory activity (47) . Their spatial and temporal distribution closely resembles cerebral blood flow, traveling from the arteries through the gray matter to the veins in about 6 seconds, similar to the time it takes for blood to pass through the brain (48). Therefore the use of simultaneous multislice acquisition protocols, for example multiband echo planar imaging , pushing the temporal resolution of MRI high enough, has become significant in removing this physiological noise from the low-frequency band (49) (50) (46) (51).

Multiple processing methods have been suggested for the extraction of sLFOs for each voxel. This study uses the Time Shift Analysis where each voxel was assigned a correlation coefficient showing the relationship between the reference signal and the time shift occurring in that voxel at each TR (repetition time) (Fig 1). So for each participant, we got a time-shift map, here we referred to them as BOLD delay maps. If the time-shift value is smaller than zero, it means the BOLD signal in this voxel has a time delay to the reference time course. If the time-shift value is larger than zero, it means the BOLD signal in this voxel precedes the reference time course (52).

The reference mentioned above can be the average signal from the entire brain (20,35,38), the healthy hemisphere (26), the major venous sinuses (20), or a recursively-generated signal (53) (29). Then a cross-correlation procedure is used to determine the delay time between this peripheral signal and the time course of each voxel in this reference signal.

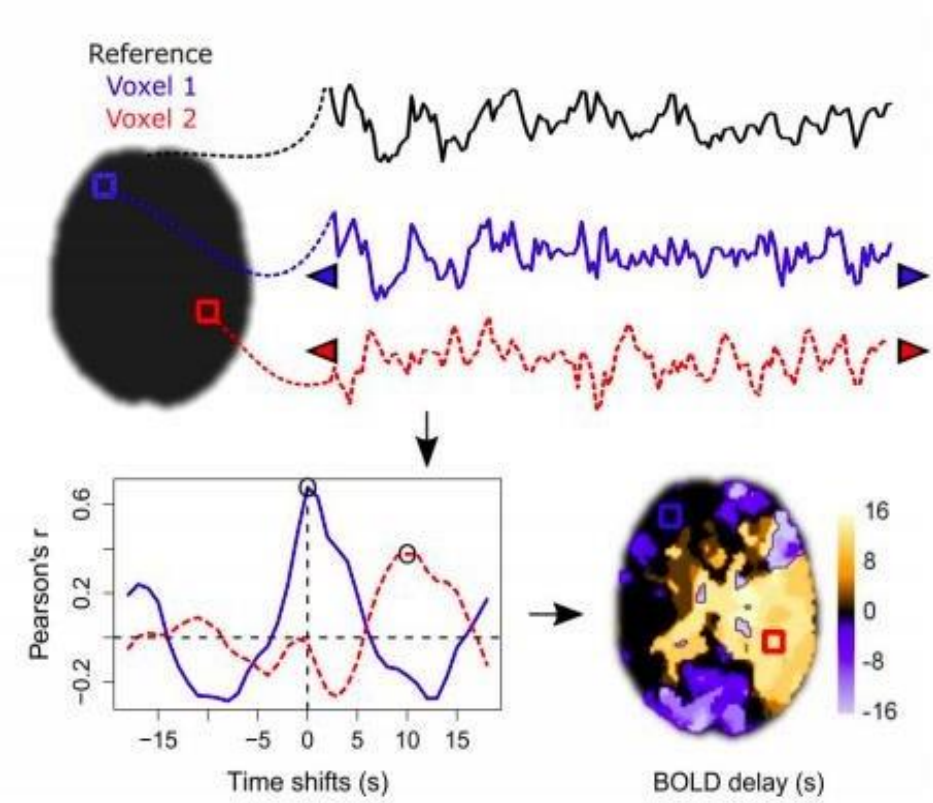

Figure 1: Illustration of the basic methodology for the time-shift analysis (TSA). For each voxel in the brain, we extracted the time course of this voxel, and then we shifted the time course, i.e. from -6.9s to +6.9s. During the shifting, we calculated the correlation coefficients between the shifted time course of each voxel and the reference time course at each TR. Then for each voxel, we identified the maximal correlation value and assigned the time-shift value which showed maximal correlation to the reference time course to this voxel. After the calculation, each voxel was assigned a value based on the time-shift required to the maximal correlation coefficient.
Reproduced from Lv et al., 2018

We created an EPI template as a reference. Resting-state EPI datasets (mean across 150 volumes) were registered to standard MNI space using FSL FLIRT (FMRIB's Linear Image Registration Tool, with 6 degrees-of-freedom) to place the images in the same orientation. The mean of these images (across patients) was used as an intermediate template, to which the original images were once again registered using an affine (12-degree-of-freedom) transformation. This procedure was performed three times and the output of the third iteration was the final EPI template (20) . We preferred a venous sinus template as a reference time series over the whole brain signal. This is because it was shown that the use of the venous sinus template has been better correlated with the perfusion maps acquired by DSC-MRI in both chronic cerebrovascular disease (38) and acute stroke (20).

sLFOs' dynamic nature has allowed scientists to apply them in the evaluation of circulation extensively. The assessment of healthy circulation using the signal in the carotid artery as a reference (32), chronic circulatory pathologies in Moyamoya patients (38), other pathologies and diseases where there are rather subtle changes in brain circulation such as Alzeihmer's disease (54) and epilepsy (55), hemodynamic changes after vessel recanalization (56) and ischemic stroke (20,26,33–36).

Imaging protocol:

In this study a Siemens *(Erlangen, Germany)* Tim Trio 3 Tesla (T) MR scanner and applied a standard stroke MRI protocol (22). The sequence parameters for the multiband EPI scan *(University of Minnesota sequence cmrr_mbep2d_bold R008* (23,24) were: [850 (resting state) time points, TR/TE=400/30 ms, flip angle 43°, matrix=64 × 64 on a 192 × 192 mm field of view (FOV), multiband factor=6, thirty 4.0 mm slices (acquisition time: 5 min 40 sec (340s)].

During the scan, patients were asked to relax, lie still, and close their eyes.

We used a multiband scan which helped scanning with high temporal resolution (57) (58). It has the advantage of allowing high-frequency cardiac and respiratory activity to be filtered out of the data.

Image preprocessing and creation of BOLD delay maps:

Preprocessing was performed on resting-state data of differing lengths in accordance with Lv et al. (26) using FSL (https://fsl.fmrib.ox.ac.uk/fsl) and AFNI (https://afni.nimh.nih.gov/afni) which comprises the removal of the first 25 volumes (10s) followed by shortening the full scan (330s) to 4 sets of source data of various scan lengths (68s, 136s, 204s, 272s), which are referred to as the 0.2, 0.4, 0.6, 0.8 scan segments respectively. Furthermore, volume realignment to the first volume, and regression of the effect of three rigid body translations and three rotations were performed. Spatial smoothing with a 6-mm gaussian kernel and band pass temporal filtering (0.01-0.15 Hz) were performed as well. Two separate metrics of head motion were calculated: mean framewise displacement (FD) and maximum FD (25) and rescaled (multiplied by 10) to increase the comparability of the measurement with the rest of the covariates in the mixed effects model.

This measure indexes the movement of the head from one volume to the next, and is calculated as the sum of the absolute values of the differentiated realignment estimates (by backwards differences) at every time point (59) . FD for the first volume of a run is 0 by convention. The purpose of this measure is to index head movement, not to precisely calculate or model it.

Rapidtide (https://github.com/bbfrederick/rapidtide)*,* for the extraction of sLFOs for each voxel, was used for the generation of BOLD delay maps. Since it was shown that the delays in acute stroke patients tend to be long, we preferred a

longer tracking range (20,56). BOLD delay maps were thresholded to 0 sec, 2.3 sec, and 4.6 sec separately. BOLD delay maps were generated from the data of each scan (Fig.2) segment for each patient and registered to an echo-planar imaging (EPI) template derived from a similar cohort of stroke patients (20,56). *AntsRegistrationSyn* script was applied (http://stnava.github.io/ANTs/) for a multi-step registration procedure (rigid → affine → deformable) (60). Double assessment methodology was used on the evaluation of the infarct lesions on the diffusion-weighted images (DWI), where they were manually delineated using MRIcro (version 1.4; Chris Rorden) by a stroke researcher and then checked by an experienced neuroradiologist. Consequently, the DWI and the delineated infarct lesions were coregistered to the same template space using ANTs (infarct lesions were masked during the registration process). Visual inspection of all the registrations then followed as a quality control measure.

Brief explanation of the comparison of BOLD delay maps at different lengths:

After having obtained the BOLD delay maps at different thresholds, we analyzed them qualitatively and quantitatively.

For the comparison of the maps quantitatively, we used Dice Similarity Coefficient (DSC) and Pearson Correlation Coefficient (PCC). The DCS is a statistical tool which measures the similarity between two sets of data. Simply put, the Dice Coefficient is 2 * the Area of Overlap divided by the total number of pixels in both images . Pearson's correlation (also called Pearson's R) is a correlation coefficient commonly used in linear regression for calculating how strong a relationship is for two variables. The result can be between +1 and -1. +1 indicates a strong positive relationship and -1 shows a strong negative relationship.

Following the calculation, a linear mixed model was executed for pair-wise comparison of the DSC value while controlling for head motion.

The hypoperfusion lesions that were defined by these BOLD delay maps were compared using Bland Altman analysis for assessing the agreement between shorter scans with the full length scan on the volumetric estimation of lesions. Bland and Altman introduced the Bland-Altman (B&A) plot to describe agreement between two quantitative measurements. They established a method to quantify agreement between two quantitative measurements by constructing limits of agreement (61). These statistical limits are calculated by using the mean and the standard deviation (*s*) of the differences between two measurements. To check the assumptions of normality of differences and other characteristics, they used a graphical approach (62). Consecutively, linear mixed effects models were used for measuring the scan length's impact on the volumetric measures of lesions.

Furthemore, we compared the maps qualitatively. We asked two expert neuroradiologists to evaluate plenty of BOLD delay maps' produced at different scan lengths. The raters were blinded to all patient data and to the length of the scans. They evaluated the interpretability of the maps with a “yes” and “no”. Furthermore, the raters were asked to assess how noisy the BOLD delay maps were (on a scale of 1 to 3, with 3 indicating the highest level of noise) and how clear certain structures such as the ventricles were on the map (on a scale of 1 to 3, with 3 indicating the highest structure clarity). We provided them with some examples on what “good” and “ bad” maps are. Based on that, they filled the excel-sheet provided. The results were furthermore assessed with inter-reader agreement using weighted Cohen's Kappa (KW) (63). Cohen's kappa is a widely used index for assessing agreement between raters. The kappa index assesses both the bias and the precision between raters' ratings which leads to a more precise calculation of the inter-rater agreement (64).

Another essential feature of an imaging technique in order for it to be used in clinical practice is its diagnostic accuracy. Therefore, the sensitivity to hypoperfusion detection of BOLD delay maps from the full-length and shorter length scans were measured separately for each reader. A binary logistic mixed model was executed for comparing hypoperfusion findings of shorter scans with the full length scan while accounting for head motion and readers

All statistical analysis was performed using *R* Statistical Software (65).

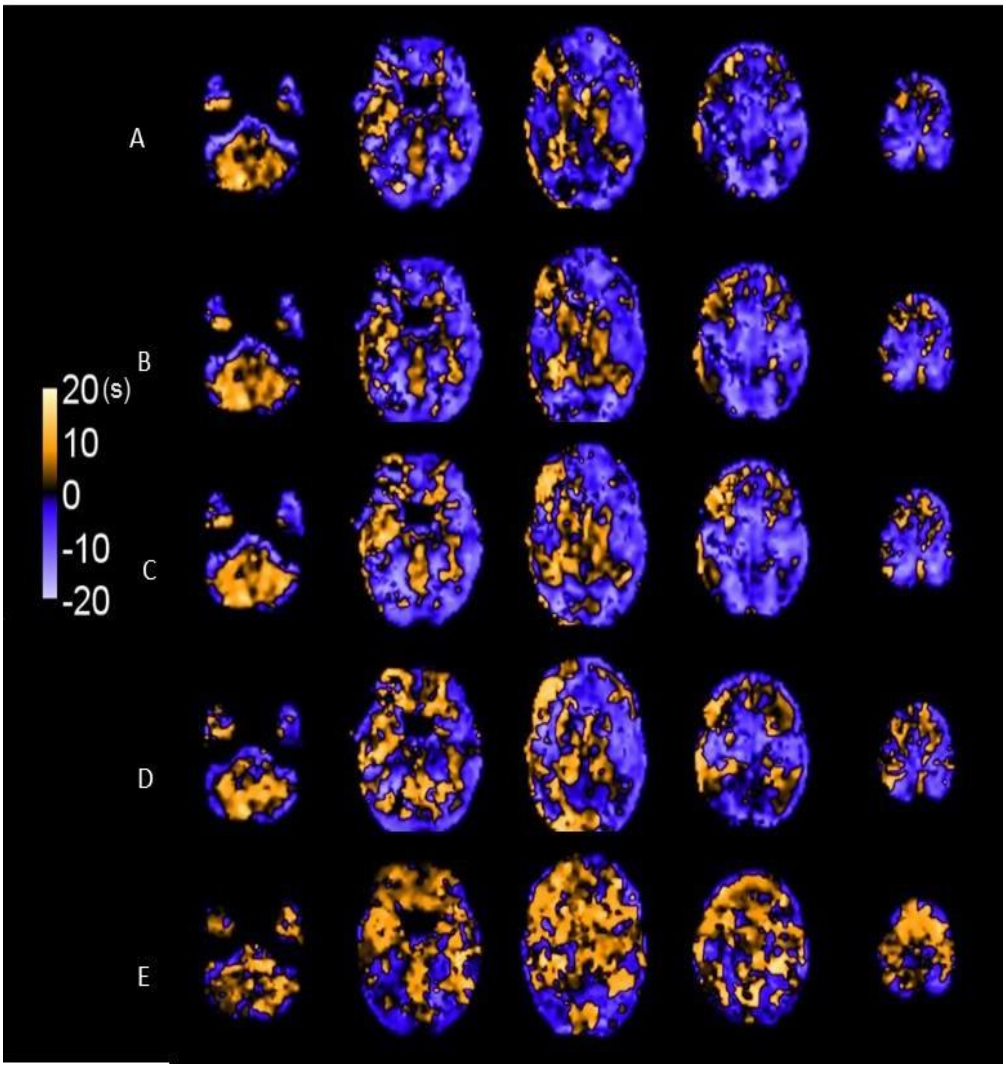

Figure 2. Examples of how the BOLD delay maps look at various scan lengths. After the removal of the first 25 volumes (10s), we shortened the full length scan which was 330s long and shown here as **A**. Substantially, 4 sets of source data of various scan lengths were produced. **B** is referred to as the 0.8 scan which is 272s long. **C** is referred to as the 0.6 scan which is 204s long. **D** is named as 0.4 scan which is 136s long, and finally **E** is the shortest scan, 0.2 scan, which is 68s. BOLD delay maps were thresholded to 0 sec, 2.3 sec, and 4.6 sec separately and registered to an echo-planar imaging (EPI) template derived from a similar cohort of stroke patients.

Reproduced by Tanritanir et al., 2020

Interpretation of the results and discussing the clinical applicability of the outcome:

When looking at the distribution of spatial overlap metrics (Dice Similarity Coefficient) between perfusion lesions from each shortened scan and perfusion lesions from the full scan, it is seen that the highest spatial overlap was between the 0.8 scan and the full scan (0.68; IQR=0.56-0.81) and it decreased with decreasing scan length, a 20% reduction in scan length decreased the Dice Coefficient by 0.15 [-0.19, -0.11]. Pearson correlation coefficient showed similar results*. (Fig 3)*

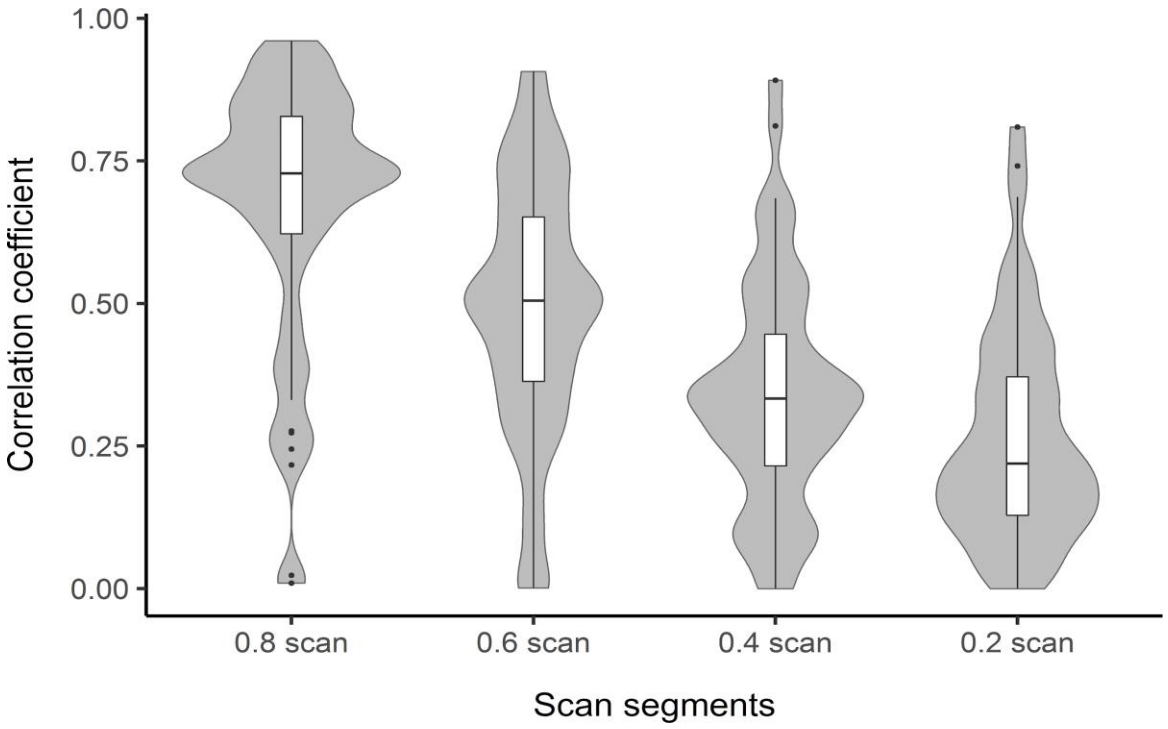

Figure 3: Violin plot of the Correlation Coefficient for spatially comparing lesions at shorter scans with that of the full length scans (220 measures of 43 individuals). 20% reduction in the scan length results in 0.17 [-0.21, -0.13] decrease in Correlation Coefficient (R^2c= 0.36, R^2m=0.7).

Applying Bland-Altmann analysis displayed that there was no systematic bias between different scan lengths in terms of detected lesion volumes, even when we accounted for head motion values using linear mixed models. *Reproduced from Tanritanir et al., 2020*

Striking outcomes were observed analyzing the diagnostic accuracy of BOLD delay maps. Shortening the scan length by 60% significantly decreased the sensitivity of the BOLD delay map to hypoperfusion (Fig.4). Odds ratios [95%CI] for the 0.4 and 0.2 scans were as follows: 0.33 [0.18, 0.59] and 0.18 [0.1, 0.32]. Furthermore, according to our readers, the quality of the maps deteriorated when reducing scan length by 60% as well. When taking head motion values into account, it was shown that the maps lost their structure clarity and interpretability and became noisier at the 0.4 and 0.2 scan lengths.

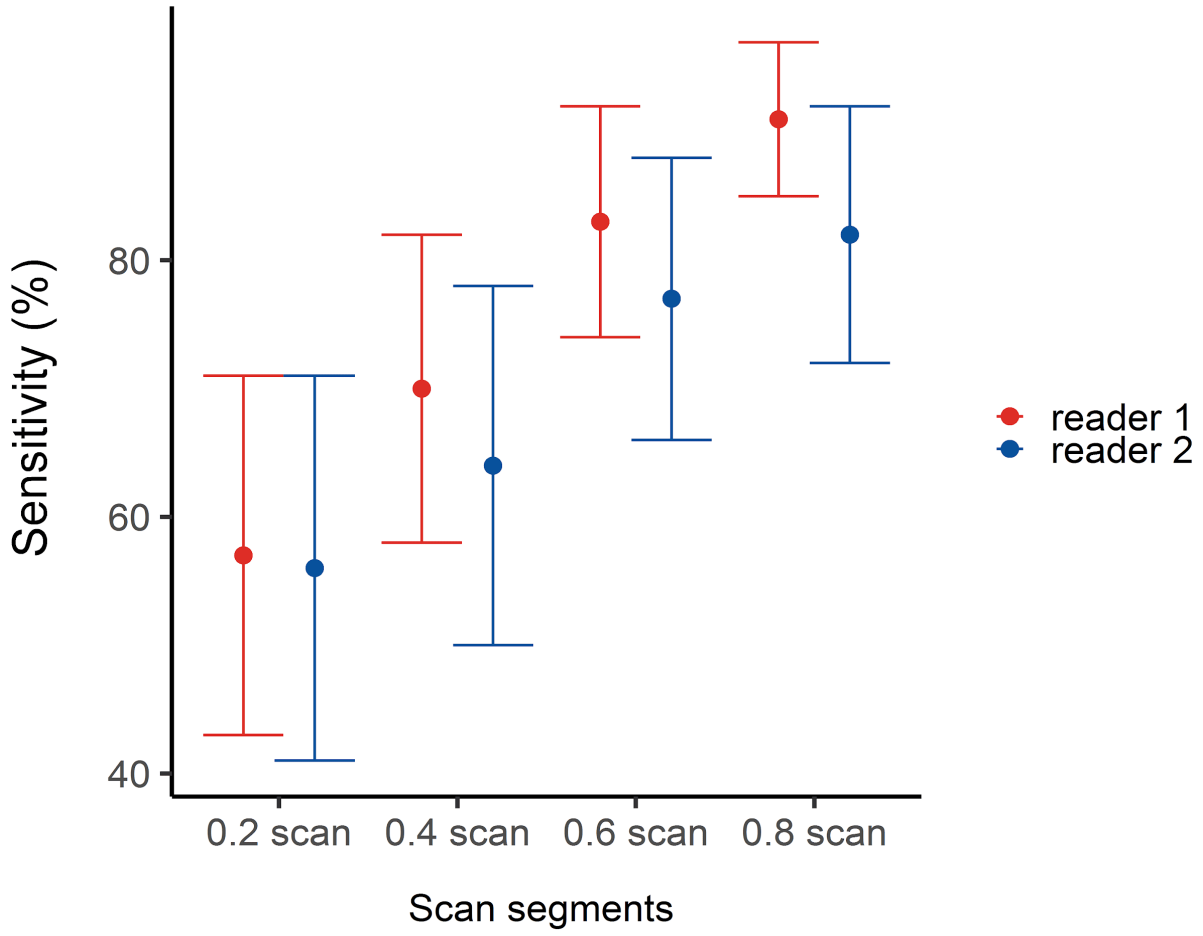

Figure 4. Sensitivity of shorter scans to detecting hypoperfusion lesions. Dots show the mean and the error bars show the 95% CI. Binary logistic mixed model (two level; random-intercept) showed that at 0.4 and 0.2 scans, the hypoperfusion detection was impaired with the odds ratio of 0.33 [0.18, 0.59] and 0.18 [0.1, 0.32] accordingly.

Reproduced from Tanritanir et al., 2020

Taking a look at our findings on the inter-reader agreement, our readers least agreed on the variables Interpretability and Structure Clarity across all scan-lengths with KW values ranging from 0.54 to 0.56 and 0.45 to 0.58 respectively.

Noiseness was consistent with the readers' ability to detect hypoperfusion, there they agreed “good” to “very good” (66) (KW: 0.62 to 0.81; 0.64 to 0.82, accordingly). A similar level of reader agreement was reached with DSC-MRI and arterial spin labeling (ASL) in terms of detecting perfusion deficits with KW values of 0.64 and 0.6 respectively, in a study on 105 patients (67). The two shortest scan segments (0.4 and 0.2 scans) were where our readers consistently agreed “good” to “very good” (KW: 0.62 to 0.83) on all five variables. The higher agreement on these quality control variables in the shortest scans may be explained by the relative ease with which the maps with the worst quality were judged by the readers. Overall, particularly for a relatively new method like BOLD delay, the inter-reader agreement in this study is within the expected range.

As our findings suggest, head motion is a significant variable deteriorating the quality of our BOLD delay maps while being highly associated with higher hypoperfusion volumes as well. The occurrence of undesired perturbations in the BOLD signal caused by head motion is a known major problem in resting-state fMRI studies. BOLD signal changes caused by head motion lead to large variations in the time courses in resting state fMRI studies (59,68–70). Head motion is regarded as the primary limiting factor for BOLD delay's use as perfusion imaging technique in a stroke workup (26). In fact, in a recent pilot study, the intra-subject reproducibility of BOLD delay values in stroke patients was found to be adversely influenced by head motion (71). In the current study, we, therefore, accounted for subject head motion in our mixed effects models of the relationship between scan length and BOLD delay map quality. The calculation of head motion was achieved by taking mean framewise

displacement (FD) (59) and the maximum FD (29). We found that mean FD significantly and adversely affected the level of noise, the structure clarity, and the volume of BOLD delay lesions independent of scan length.

In order to reduce head motion in an appropriate and reliable way, we could take a look at functional connectivity studies where this issue has been addressed. Multiple ways on how to tackle it have been suggested; scrubbing, which effectively removes volumes with high motion, has shown promise (59). However, for this to be applicable to BOLD delay studies on the detection of hypoperfusion, we need to know the minimum amount of data which is adequate after the removal of high-motion volumes. A scan length of 15 - 30 minutes has been suggested in functional connectivity studies of stroke patients (69). Our findings demonstrate that much less data may be required for sufficient detection of hypoperfusion in acute stroke. A systematic analysis of the impact of scan length on BOLD delay can allow the application of real-time motion monitoring approaches, where scans can run until a sufficient amount of low-motion data is acquired (72).

Here we presented a systematic investigation among patients with ischemic stroke of the effects of scan duration on the evaluation of brain perfusion using BOLD delay. Our study suggests that our initial, full-length scan, 5 min and 40 sec, can be reduced down to 3 min and 24 sec without a critical loss of diagnostic accuracy and image quality of BOLD delay maps, even when taking head motion into account. A scan duration as short as 1 min and 8 sec was robust for estimating hypoperfusion lesion volume, which holds substantial importance for the approximation of the ischemic penumbra using MR-based perfusion-diffusion mismatch (73). This area, defined as the mismatch between infarcted tissue shown by diffusion-weighted imaging (DWI) and hypoperfused tissue shown by perfusion imaging, is an early marker for tissue at risk (74).

A reduction of a scan-length by nearly 40% holds great importance considering that acute stroke is an emergency where decision making has to be done very quickly. A time gain of about two and a half minutes per patient would bring significant efficiency in various perspectives. Faster scanning means better use of resources and better network performance. When scans are shorter, patient compliance will also be higher. This overall will bring higher competency to the clinical setting. More accurate preliminary diagnosis will be made. This would also lead to less workload in the various teams engaged in the treatment of the patient.

These findings are overall in accordance with reports released prior to our study. Lv et al. (52) researched the correlation between the areas of BOLD signal delay and areas of hypoperfusion identified by DSC-MRI in acute stroke patients. BOLD delay maps acquired in 3 min and 4 sec provided similar information to that of the full length scan (5 min 50 sec) in terms of spatial overlap with the MTT lesion of the subject. Christen et al. (38) showed that BOLD delay maps of Moyamoya patients produced at a shorter scan-length (3 min 36 sec) exhibit high correlation with the Tmax maps of the subjects. However, a systematic evaluation of scan shortening and its impacts on various, especially clinical, aspects was lacking in both these studies.

It is very appealing to discuss what's next. This dissertation can be the initial approach for shortening the scans. Can we make scans even shorter? Theoretically, yes. The more precise ways we develop to shorten the scans, the better denoising strategies we will achieve. As explained above, head motion correction goes hand-in-hand with shortening of the scans. Head motion could indirectly reduce as we cut the duration the patient spends in the MRI. Furthermore, we could get better at removing the “non-interesting” signal sources which, as mentioned above, are faster signals and that easily alias in the signals we are interested in. Post-processing strategies will also advance when

we have less noise as a result of better head motion correction.

Our study has a few limitations. We only had a small subset of patients who received a DSC-MRI as well, not allowing us to make an adequate comparison of the shorter BOLD delay scans with an established perfusion method. This was mainly because of the restrictions mentioned by the European Medicines Agency on the use of gadolinium-based contrast agents (75). Secondly, it should be kept in mind that the results of this study depend on the exact sequence parameters (e.g. TR, TE, spatial resolution). Different minimum acceptable scan times may apply to sequences with different parameters. Furthermore, we do not yet know the possible advantages of scan times longer than what is implemented in the current study (5 min 40 sec). However, such scans most probably would not be suitable in emergency situations, such as acute stroke.

BOLD delay scans, which allow the assessment of hypoperfusion without exogenous contrast agents, can be shortened by up to 40% compared to currently implemented scans. This reduces the effect of one of the major problems hindering the use of BOLD delay imaging on a daily basis in the clinic: patient motion. Furthermore, time-effectiveness is undeniably desirable when there is a clinical emergency, and these shortened scans may lead to quicker decision-making in acute stroke. These results demonstrate a very exciting and promising step towards quicker and contrast-agent-free assessment of perfusion in acute stroke patients.

Bibliography

1. Aho K, Harmsen P, Hatano S, Marquardsen J, Smirnov VE, Strasser T. Cerebrovascular disease in the community: results of a WHO collaborative study. Bull World Health Organ. 1980;58(1):113–30.
2. Sacco RL, Kasner SE, Broderick JP, Caplan LR, Connors JJB, Culebras A, et al. An updated definition of stroke for the 21st century: a statement for healthcare professionals from the American Heart Association/American Stroke Association. Stroke. 2013 Jul;44(7):2064–89.
3. GBD 2016 Disease and Injury Incidence and Prevalence Collaborators. Global, regional, and national incidence, prevalence, and years lived with disability for 328 diseases and injuries for 195 countries, 1990-2016: a systematic analysis for the Global Burden of Disease Study 2016. Lancet. 2017 Sep 16;390(10100):1211–59.
4. Plass D, Vos T, Hornberg C, Scheidt-Nave C, Zeeb H, Krämer A. Trends in disease burden in Germany: results, implications and limitations of the Global Burden of Disease study. Dtsch Arztebl Int. 2014 Sep 19;111(38):629–38.
5. Kuriakose D, Xiao Z. Pathophysiology and treatment of stroke: present status and future perspectives. Int J Mol Sci. 2020 Oct 15;21(20).
6. Broughton BRS, Reutens DC, Sobey CG. Apoptotic mechanisms after cerebral ischemia. Stroke. 2009 May;40(5):e331-9.
7. GBD 2013 Mortality and Causes of Death Collaborators. Global, regional, and national age-sex specific all-cause and cause-specific mortality for 240 causes of death, 1990-2013: a systematic analysis for the Global Burden of Disease Study 2013. Lancet. 2015 Jan 10;385(9963):117–71.
8. Flaherty ML, Woo D, Haverbusch M, Sekar P, Khoury J, Sauerbeck L, et al. Racial variations in location and risk of intracerebral hemorrhage. Stroke. 2005 May;36(5):934–7.
9. Muir KW, Buchan A, von Kummer R, Rother J, Baron J-C. Imaging of acute stroke. Lancet Neurol. 2006 Sep;5(9):755–68.
10. Hacke W, Schwab S, Horn M, Spranger M, De Georgia M, von Kummer R. “Malignant” middle cerebral artery territory infarction: clinical course and prognostic signs. Arch Neurol. 1996 Apr;53(4):309–15.
11. Liebeskind DS, Jüttler E, Shapovalov Y, Yegin A, Landen J, Jauch EC. Cerebral edema associated with large hemispheric infarction. Stroke. 2019 Sep;50(9):2619–25.
12. Neumann-Haefelin T, Kastrup A, de Crespigny A, Yenari MA, Ringer T, Sun GH, et al. Serial MRI after transient focal cerebral ischemia in rats: dynamics of tissue injury, blood-brain barrier damage, and edema formation. Stroke. 2000 Aug;31(8):1965–72; discussion 1972.
13. Fiebach JB, Schellinger PD, Gass A, Kucinski T, Siebler M, Villringer A, et al. Stroke magnetic resonance imaging is accurate in hyperacute intracerebral hemorrhage: a multicenter study on the validity of stroke imaging. Stroke. 2004 Feb;35(2):502–6.

14. Wardlaw JM, Mielke O. Early signs of brain infarction at CT: observer reliability and outcome after thrombolytic treatment--systematic review. Radiology. 2005 May;235(2):444–53.

15. Fiebach JB, Schellinger PD, Jansen O, Meyer M, Wilde P, Bender J, et al. CT and diffusion-weighted MR imaging in randomized order: diffusion-weighted imaging results in higher accuracy and lower interrater variability in the diagnosis of hyperacute ischemic stroke. Stroke. 2002 Sep;33(9):2206–10.

16. Warach S, Gaa J, Siewert B, Wielopolski P, Edelman RR. Acute human stroke studied by whole brain echo planar diffusion-weighted magnetic resonance imaging. Ann Neurol. 1995 Feb;37(2):231–41.

17. Chalela JA, Kidwell CS, Nentwich LM, Luby M, Butman JA, Demchuk AM, et al. Magnetic resonance imaging and computed tomography in emergency assessment of patients with suspected acute stroke: a prospective comparison. Lancet. 2007 Jan 27;369(9558):293–8.

18. Leigh R, Knutsson L, Zhou J, van Zijl PC. Imaging the physiological evolution of the ischemic penumbra in acute ischemic stroke. J Cereb Blood Flow Metab. 2018 Sep;38(9):1500–16.

19. Hotter B, Ostwaldt A-C, Levichev-Connolly A, Rozanski M, Audebert HJ, Fiebach JB. Natural course of total mismatch and predictors for tissue infarction. Neurology. 2015 Sep 1;85(9):770–5.

20. Khalil AA, Ostwaldt A-C, Nierhaus T, Ganeshan R, Audebert HJ, Villringer K, et al. Relationship Between Changes in the Temporal Dynamics of the Blood-Oxygen-Level-Dependent Signal and Hypoperfusion in Acute Ischemic Stroke. Stroke. 2017 Mar 8;48(4):925–31.

21. Campbell BCV, Macrae IM. Translational perspectives on perfusion-diffusion mismatch in ischemic stroke. Int J Stroke. 2015 Feb;10(2):153–62.

22. Khawaja AZ, Cassidy DB, Al Shakarchi J, McGrogan DG, Inston NG, Jones RG. Revisiting the risks of MRI with Gadolinium based contrast agents-review of literature and guidelines. Insights Imaging. 2015 Oct;6(5):553–8.

23. Gulani V, Calamante F, Shellock FG, Kanal E, Reeder SB, International Society for Magnetic Resonance in Medicine. Gadolinium deposition in the brain: summary of evidence and recommendations. Lancet Neurol. 2017 Jul;16(7):564–70.

24. Donahue MJ, Juttukonda MR, Watchmaker JM. Noise concerns and post-processing procedures in cerebral blood flow (CBF) and cerebral blood volume (CBV) functional magnetic resonance imaging. Neuroimage. 2017 Jul 1;154:43–58.

25. Zaharchuk G. Arterial spin labeling for acute stroke: practical considerations. Transl Stroke Res. 2012 Jun;3(2):228–35.

26. Lv Y, Margulies DS, Cameron Craddock R, Long X, Winter B, Gierhake D, et al. Identifying the perfusion deficit in acute stroke with resting-state functional magnetic resonance imaging. Ann Neurol. 2013 Jan;73(1):136–40.

27. Tong Y, Frederick BD. Time lag dependent multimodal processing of concurrent fMRI and near-infrared spectroscopy (NIRS) data suggests a global circulatory origin for low-frequency oscillation signals in human brain. Neuroimage. 2010 Nov 1;53(2):553–64.

28. Tong Y, Hocke LM, Licata SC, Frederick B deB. Low-frequency oscillations measured in the periphery with near-infrared spectroscopy are strongly correlated with blood oxygen level-dependent functional magnetic resonance imaging signals. J Biomed Opt. 2012 Oct;17(10):106004.

29. Tong Y, Frederick B deB. Tracking cerebral blood flow in BOLD fMRI using recursively generated regressors. Hum Brain Mapp. 2014 Nov;35(11):5471–85.

30. Tong Y, Hocke LM, Lindsey KP, Erdoğan SB, Vitaliano G, Caine CE, et al. Systemic Low-Frequency Oscillations in BOLD Signal Vary with Tissue Type. Front Neurosci. 2016 Jun 30;10:313.

31. Tong Y, Lindsey KP, Hocke LM, Vitaliano G, Mintzopoulos D, Frederick B deB. Perfusion information extracted from resting state functional magnetic resonance imaging. J Cereb Blood Flow Metab. 2017 Feb;37(2):564–76.

32. Tong Y, Yao JF, Chen JJ, Frederick B deB. The resting-state fMRI arterial signal predicts differential blood transit time through the brain. J Cereb Blood Flow Metab. 2019;39(6):1148–60.

33. Amemiya S, Kunimatsu A, Saito N, Ohtomo K. Impaired hemodynamic response in the ischemic brain assessed with BOLD fMRI. Neuroimage. 2012 Jul 2;61(3):579–90.

34. Ni L, Li J, Li W, Zhou F, Wang F, Schwarz CG, et al. The value of resting-state functional MRI in subacute ischemic stroke: comparison with dynamic susceptibility contrast-enhanced perfusion MRI. Sci Rep. 2017 Jan 31;7:41586.

35. Siegel JS, Snyder AZ, Ramsey L, Shulman GL, Corbetta M. The effects of hemodynamic lag on functional connectivity and behavior after stroke. J Cereb Blood Flow Metab. 2016;36(12):2162–76.

36. Chen Q, Zhou J, Zhang H, Chen Y, Mao C, Chen X, et al. One-step analysis of brain perfusion and function for acute stroke patients after reperfusion: A resting-state fMRI study. J Magn Reson Imaging. 2019;50(1):221–9.

37. Lv Y, Wei W, Song Y, Han Y, Zhou C, Zhou D, et al. Non-invasive evaluation of cerebral perfusion in patients with transient ischemic attack: an fMRI study. J Neurol. 2019 Jan;266(1):157–64.

38. Christen T, Jahanian H, Ni WW, Qiu D, Moseley ME, Zaharchuk G. Noncontrast mapping of arterial delay and functional connectivity using resting-state functional MRI: a study in Moyamoya patients. J Magn Reson Imaging. 2015 Feb;41(2):424–30.

39. De Vis JB, Bhogal AA, Hendrikse J, Petersen ET, Siero JCW. Effect sizes of BOLD CVR, resting-state signal fluctuations and time delay measures for the assessment of hemodynamic impairment in carotid occlusion patients. Neuroimage. 2018 Oct 1;179:530–9.

40. Wu J, Dehkharghani S, Nahab F, Allen J, Qiu D. The Effects of Acetazolamide on the

Evaluation of Cerebral Hemodynamics and Functional Connectivity Using Blood Oxygen Level-Dependent MR Imaging in Patients with Chronic Steno-Occlusive Disease of the Anterior Circulation. AJNR Am J Neuroradiol. 2017;38(1):139–45.

41. Qian T, Zanchi D, Rodriguez C, Ackermann M, Giannakopoulos P, Haller S. Detecting Perfusion Pattern Based on the Background Low-Frequency Fluctuation in Resting-State Functional Magnetic Resonance Imaging Data and Its Influence on Resting-State Networks: An Iterative Postprocessing Approach. Brain Connect. 2017;7(10):627–34.
42. Josephs O, Henson RN. Event-related functional magnetic resonance imaging: modelling, inference and optimization. Philos Trans R Soc Lond B Biol Sci. 1999 Jul 29;354(1387):1215–28.
43. Logothetis NK, Pauls J, Augath M, Trinath T, Oeltermann A. Neurophysiological investigation of the basis of the fMRI signal. Nature. 2001 Jul 12;412(6843):150–7.
44. Liu TT. Reprint of “Noise contributions to the fMRI signal: An Overview”. Neuroimage. 2017 Jul 1;154:4–14.
45. Erdoğan SB, Tong Y, Hocke LM, Lindsey KP, deB Frederick B. Correcting for Blood Arrival Time in Global Mean Regression Enhances Functional Connectivity Analysis of Resting State fMRI-BOLD Signals. Front Hum Neurosci. 2016 Jun 28;10:311.
46. Birn RM, Diamond JB, Smith MA, Bandettini PA. Separating respiratory-variation-related fluctuations from neuronal-activity-related fluctuations in fMRI. Neuroimage. 2006 Jul 15;31(4):1536–48.
47. Liu TT. Noise contributions to the fMRI signal: An overview. Neuroimage. 2016 Dec;143:141–51.
48. Crandell D, Moinuddin M, Fields M, Friedman BI, Robertson J. Cerebral transit time of 99m technetium sodium pertechnetate before and after cerebral arteriography. J Neurosurg. 1973 May;38(5):545–7.
49. Glover GH, Li TQ, Ress D. Image-based method for retrospective correction of physiological motion effects in fMRI: RETROICOR. Magn Reson Med. 2000 Jul;44(1):162–7.
50. Chang C, Glover GH. Effects of model-based physiological noise correction on default mode network anti-correlations and correlations. Neuroimage. 2009 Oct 1;47(4):1448–59.
51. Birn RM, Smith MA, Jones TB, Bandettini PA. The respiration response function: the temporal dynamics of fMRI signal fluctuations related to changes in respiration. Neuroimage. 2008 Apr 1;40(2):644–54.
52. Lv Y. Application of resting-state fMRI methods to acute ischemic stroke [Internet] [Doctoral dissertation]. 2013 [cited 2019 Feb 26]. Available from: http://www.qucosa.de/fileadmin/data/qucosa/documents/12691/PhD%20Thesis_lv.pdf
53. Aso T, Jiang G, Urayama S-I, Fukuyama H. A Resilient, Non-neuronal Source of the Spatiotemporal Lag Structure Detected by BOLD Signal-Based Blood Flow Tracking. Front Neurosci. 2017 May 11;11:256.
54. Yan S, Qi Z, An Y, Zhang M, Qian T, Lu J. Detecting perfusion deficit in Alzheimer's disease and mild cognitive impairment patients by resting-state fMRI. J Magn Reson

Imaging. 2019;49(4):1099–104.

55. Shah MN, Mitra A, Goyal MS, Snyder AZ, Zhang J, Shimony JS, et al. Resting state signal latency predicts laterality in pediatric medically refractory temporal lobe epilepsy. Childs Nerv Syst. 2018 May;34(5):901–10.

56. Khalil AA, Villringer K, Filleböck V, Hu J-Y, Rocco A, Fiebach JB, et al. Non-invasive monitoring of longitudinal changes in cerebral hemodynamics in acute ischemic stroke using BOLD signal delay. J Cereb Blood Flow Metab. 2020;40(1):23–34.

57. Xu J, Moeller S, Auerbach EJ, Strupp J, Smith SM, Feinberg DA, et al. Evaluation of slice accelerations using multiband echo planar imaging at 3 T. Neuroimage. 2013 Dec;83:991–1001.

58. Feinberg DA, Moeller S, Smith SM, Auerbach E, Ramanna S, Gunther M, et al. Multiplexed echo planar imaging for sub-second whole brain FMRI and fast diffusion imaging. PLoS ONE. 2010 Dec 20;5(12):e15710.

59. Power JD, Barnes KA, Snyder AZ, Schlaggar BL, Petersen SE. Spurious but systematic correlations in functional connectivity MRI networks arise from subject motion. Neuroimage. 2012 Feb 1;59(3):2142–54.

60. Tustison NJ, Avants BB. Explicit B-spline regularization in diffeomorphic image registration. Front Neuroinformatics. 2013 Dec 23;7:39.

61. Bland JM, Altman DG. Measuring agreement in method comparison studies. Stat Methods Med Res. 1999 Jun;8(2):135–60.

62. Giavarina D. Understanding Bland Altman analysis. Biochem Med (Zagreb). 2015 Jun 5;25(2):141–51.

63. Cohen J. A Coefficient of Agreement for Nominal Scales. Educ Psychol Meas. 1960 Apr 1;20(1):37–46.

64. Tang W, Hu J, Zhang H, Wu P, He H. Kappa coefficient: a popular measure of rater agreement. Shanghai Arch Psychiatry. 2015 Feb 25;27(1):62–7.

65. R Core Team. R: A Language and Environment for Statistical Computing. Vienna, Austria: R Foundation for Statistical Computing; 2017.

66. Fleiss JL, Cohen J, Everitt BS. Large sample standard errors of kappa and weighted kappa. Psychol Bull. 1969;72(5):323–7.

67. Bokkers RPH, Hernandez DA, Merino JG, Mirasol RV, van Osch MJ, Hendrikse J, et al. Whole-brain arterial spin labeling perfusion MRI in patients with acute stroke. Stroke. 2012 May;43(5):1290–4.

68. Reuter M, Tisdall MD, Qureshi A, Buckner RL, van der Kouwe AJW, Fischl B. Head motion during MRI acquisition reduces gray matter volume and thickness estimates. Neuroimage. 2015 Feb 15;107:107–15.

69. Siegel JS, Mitra A, Laumann TO, Seitzman BA, Raichle M, Corbetta M, et al. Data quality influences observed links between functional connectivity and behavior. Cereb Cortex. 2017 Sep 1;27(9):4492–502.

70. Van Dijk KRA, Sabuncu MR, Buckner RL. The influence of head motion on intrinsic functional connectivity MRI. Neuroimage. 2012 Jan 2;59(1):431–8.

71. Khalil AA, Tanritanir AC, Grittner U, Villringer A, Fiebach JB, Mekle R. Reproducibility of BOLD delay perfusion measurements in acute stroke patients. Proceedings of the 26th Annual Meeting of ISMRM, Paris, 2017.; 2018.

72. Dosenbach NUF, Koller JM, Earl EA, Miranda-Dominguez O, Klein RL, Van AN, et al. Real-time motion analytics during brain MRI improve data quality and reduce costs. Neuroimage. 2017 Nov 1;161:80–93.

73. Heit JJ, Zaharchuk G, Wintermark M. Advanced neuroimaging of acute ischemic stroke: penumbra and collateral assessment. Neuroimaging Clin N Am. 2018 Nov;28(4):585–97.

74. Baird AE, Benfield A, Schlaug G, Siewert B, Lövblad KO, Edelman RR, et al. Enlargement of human cerebral ischemic lesion volumes measured by diffusion-weighted magnetic resonance imaging. Ann Neurol. 1997 May;41(5):581–9.

75. European Medicines Agency. Gadolinium-containing contrast agents . European Medicines Agency; 2017 Jul.

EIDESSTATTLICHE VERSICHERUNG

„Ich, Ayse Ceren Tanritanir, versichere an Eides statt durch meine eigenhändige Unterschrift, dass ich die vorgelegte Dissertation mit dem Thema: *How short can we go? The impact of BOLD delay scan length on detecting hypoperfusion. Wie kurz darf es sein? Der Einfluss der BOLD Delay Scan Länge auf die Erkennung von Hypoperfusionen*
selbstständig und ohne nicht offengelegte Hilfe Dritter verfasst und keine anderen als die angegebenen Quellen und Hilfsmittel genutzt habe."

Alle Stellen, die wörtlich oder dem Sinne nach auf Publikationen oder Vorträgen anderer Autoren beruhen, sind als solche in korrekter Zitierung kenntlich gemacht. Die Abschnitte zu Methodik (insbesondere praktische Arbeiten, Laborbestimmungen, statistische Aufarbeitung) und Resultaten (insbesondere Abbildungen, Graphiken und Tabellen) werden von mir verantwortet.

Ich versichere ferner, dass ich die in Zusammenarbeit mit anderen Personen generierten Daten, Datenauswertungen und Schlussfolgerungen korrekt gekennzeichnet und meinen eigenen Beitrag sowie die Beiträge anderer Personen korrekt kenntlich gemacht habe (siehe Anteilserklärung). Texte oder Textteile, die gemeinsam mit anderen erstellt oder verwendet wurden, habe ich korrekt kenntlich gemacht.

Meine Anteile an etwaigen Publikationen zu dieser Dissertation entsprechen denen, die in der untenstehenden gemeinsamen Erklärung mit dem/der Erstbetreuer/in, angegeben sind. Für sämtliche im Rahmen der Dissertation entstandenen Publikationen wurden die Richtlinien des ICMJE (International Committee of Medical Journal Editors; www.icmje.og) zur Autorenschaft eingehalten. Ich erkläre ferner, dass mir die Satzung der Charité – Universitätsmedizin Berlin zur Sicherung Guter Wissenschaftlicher Praxis bekannt ist und ich mich zur Einhaltung dieser Satzung verpflichte.

Weiterhin versichere ich, dass ich diese Dissertation weder in gleicher noch in ähnlicher Form bereits an einer anderen Fakultät eingereicht habe.

Die Bedeutung dieser eidesstattlichen Versicherung und die strafrechtlichen Folgen einer unwahren eidesstattlichen Versicherung (§§156, 161 des Strafgesetzbuches) sind mir bekannt und bewusst."

Datum: _____ Unterschrift

Ausführliche Anteilserklärung an der erfolgten Publikation

Ayse Ceren Tanritanir, Kersten Villringer , Ivana Galinovic , Ulrike Grittner , Evgeniya Kirilina , Jochen B. Fiebach, Arno Villringer , Ahmed A. Khalil, The effect of scan length on the assessment of perfusion using BOLD delay in ischemic stroke, Frontiers in Neurology, 2020

Beitrag im Einzelnen

- Ich habe meine Forschung mit Unterweisung in den Grundlagen der medizinischen Bildaufnahme/Verarbeitung (MRT-Physik, MATLAB) begonnen.

- Ich war selbständig bei Sammlung und Extraktion der MULTIBAND Resting State Daten sowie Daten von den anderen Sequenzen des Standardprotokolls für die Schlaganfallbildgebung im Laufe des Projekts.

- Ich habe mit Hilfe meinen Betreuern die Studiendaten nach Ein- und Ausschlusskriterien geprüft. Das grosse Teil des Lesen von Diffusions- und Perfusionsbildern, Abgrenzung der Infarktläsionen in den Diffusionsbildern und Registrierung der ausgewählten Perfusionsbilder habe ich alleine gemacht.

- Ich mit Hilfe meiner Betreuern habe die Qualitätskontrolle und Vorverarbeitung der Studiendaten mit MRT-Bild Analyse, SPM, FSL gemacht.

- Mir wurde die Grundlage der Bildanalyse der Resting State Daten mit Nutzung der “Time-Shift-Analysis" beigebracht. Zusätzlich dazu erfolgten die Volumetrische Rechnung der Hypoperfusion Läsionen, Vorbereitung der Qualitativen Analyse (Auswertung durch 2 Radiologen) von BOLD Delay Maps. Aus dieser ist die ergänzende Abbildung 2 entstanden. Anschliessend sind die Auswertungen analysiert worden. Aus dieser Analyse ist die ergänzende Tabelle 2 entstanden.

- Ich habe bei meiner statistischen Analyse das Programm RStudio benutzt und dabei Unterstützung von unserer Statistikern im Institut bekommen. Aus meiner statistischen Auswertung sind die Tabelle 2-3 sowie Abbildungen 1,2,34,5,6 entstanden.“

- Interpretation der Daten und Bewertung mit den Betreuern.

- Ich habe eine ausführliche online Recherche der bereits publizierten Studien gemacht, vor allem bezüglich der Abkürzung der Scan Länge. Aus meiner Recherche ist ein Teil von der Tabelle 1 entstanden.
- Planung des Manuskripts mit grosser Hilfe meinen Betreuern.

- Ich habe das Grundlage des Manuskriptes geschrieben und Dr. Khalil hat bei der Finalisierung und Verbesserung des Manuskriptes enorm geholfen. Wir haben Kommentare, Korrekturen und Ergänzungen durch alle Autoren bekommen.

_____

Unterschrift, Datum und Stempel des/der erstbetreuenden Hochschullehrers/in

_____

Unterschrift des Doktoranden/der Doktorandin

Journal Data Filtered By: Selected JCR Year: 2018 Selected Editions: SCIE,SSCI Selected Categories: "CLINICAL NEUROLOGY" Selected Category
Scheme: WoS
Gesamtanzahl: 199 Journale

Rank	Full Journal Title	Total Cites	Journal Impact Factor	Eigenfactor Score
1	LANCET NEUROLOGY	30,748	28.755	0.069460
2	Nature Reviews Neurology	9,548	21.155	0.031060
3	ACTA NEUROPATHOLOGICA	20,206	18.174	0.041660
4	Alzheimers & Dementia	13,341	14.423	0.036340
5	JAMA Neurology	8,683	12.321	0.042040
6	BRAIN	52,970	11.814	0.074030
7	SLEEP MEDICINE REVIEWS	6,920	10.517	0.010920
8	NEURO-ONCOLOGY	11,858	10.091	0.029150
9	ANNALS OF NEUROLOGY	37,336	9.496	0.048630
10	NEUROLOGY	89,258	8.689	0.115200
11	JOURNAL OF NEUROLOGY NEUROSURGERY AND PSYCHIATRY	29,660	8.272	0.030730
12	MOVEMENT DISORDERS	26,964	8.061	0.037650
13	Neurology-Neuroimmunology & Neuroinflammation	1,996	7.353	0.008220
14	Brain Stimulation	5,457	6.919	0.014470
15	Epilepsy Currents	799	6.909	0.001560
16	NEUROPATHOLOGY AND APPLIED NEUROBIOLOGY	3,876	6.878	0.006420
17	NEUROSCIENTIST	4,986	6.791	0.008520
18	BRAIN PATHOLOGY	5,263	6.155	0.007880
19	Alzheimers Research & Therapy	3,160	6.142	0.010700
20	STROKE	64,814	6.046	0.082630

Rank	Full Journal Title	Total Cites	Journal Impact Factor	Eigenfactor Score
21	PAIN	38,312	6.029	0.039070
22	Translational Stroke Research	1,955	5.847	0.004330
23	Multiple Sclerosis Journal	11,501	5.649	0.022750
24	Journal of Stroke	925	5.571	0.003580
25	EPILEPSIA	26,492	5.562	0.033400
26	Neurotherapeutics	4,475	5.552	0.009060
27	JOURNAL OF PAIN	10,405	5.424	0.018280
28	BIPOLAR DISORDERS	5,143	4.936	0.006760
29	Annals of Clinical and Translational Neurology	1,858	4.656	0.008750
30	CURRENT OPINION IN NEUROLOGY	5,290	4.647	0.009650
31	NEUROSURGERY	29,096	4.605	0.020730
32	SLEEP	21,434	4.571	0.024240
33	EUROPEAN NEUROPSYCHOPHARMACOLOGY	7,488	4.468	0.015500
34	International Journal of Stroke	4,172	4.466	0.015210
35	CEPHALALGIA	9,983	4.438	0.014480
36	EUROPEAN JOURNAL OF NEUROLOGY	10,488	4.387	0.016970
37	PARKINSONISM & RELATED DISORDERS	9,119	4.360	0.018810
38	PROGRESS IN NEURO-PSYCHOPHARMACOLOGY & BIOLOGICAL PSYCHIATRY	10,674	4.315	0.012400
39	JOURNAL OF PSYCHOPHARMACOLOGY	6,460	4.221	0.010120
40	INTERNATIONAL JOURNAL OF NEUROPSYCHOPHARMACOLOGY	6,551	4.207	0.012320
41	JOURNAL OF NEUROLOGY	14,910	4.204	0.024550
42	CNS DRUGS	4,602	4.192	0.007190

Rank	Full Journal Title	Total Cites	Journal Impact Factor	Eigenfactor Score
43	JOURNAL OF NEUROSURGERY	36,001	4.130	0.027880
44	JOURNAL OF AFFECTIVE DISORDERS	30,314	4.084	0.052950
45	CNS SPECTRUMS	2,368	3.940	0.003340
46	JOURNAL OF HEADACHE AND PAIN	3,308	3.918	0.007210
47	NEUROGASTROENTEROLOGY AND MOTILITY	8,314	3.803	0.014510
48	NEUROREHABILITATION AND NEURAL REPAIR	5,071	3.757	0.008480
49	JOURNAL OF NEUROTRAUMA	14,754	3.754	0.019770
50	HEADACHE	7,897	3.749	0.009930
51	CLINICAL NEUROPHYSIOLOGY	19,574	3.675	0.021420
52	Journal of Neurodevelopmental Disorders	1,253	3.590	0.003420
53	Therapeutic Advances in Neurological Disorders	1,148	3.580	0.002760
54	Current Treatment Options in Neurology	1,200	3.574	0.002790
55	DEVELOPMENTAL MEDICINE AND CHILD NEUROLOGY	12,256	3.532	0.013840
56	Brain Tumor Pathology	739	3.509	0.001470
57	PSYCHIATRY AND CLINICAL NEUROSCIENCES	3,720	3.489	0.004230
58	JOURNAL OF NEUROPATHOLOGY AND EXPERIMENTAL NEUROLOGY	9,205	3.460	0.007510
59	Journal of Clinical Sleep Medicine	6,094	3.456	0.011390
60	Expert Review of Neurotherapeutics	4,057	3.453	0.006360
61	JOURNAL OF SLEEP RESEARCH	5,432	3.432	0.007450
62	Current Neurology and Neuroscience Reports	3,004	3.400	0.007210
63	JOURNAL OF PAIN AND SYMPTOM MANAGEMENT	11,229	3.378	0.015750
64	SLEEP MEDICINE	10,218	3.360	0.017130

Rank	Full Journal Title	Total Cites	Journal Impact Factor	Eigenfactor Score
65	AMERICAN JOURNAL OF NEURORADIOLOGY	23,231	3.256	0.028010
66	Current Alzheimer Research	4,026	3.211	0.005930
67	Spine Journal	9,595	3.196	0.019800
68	EUROPEAN ARCHIVES OF PSYCHIATRY AND CLINICAL NEUROSCIENCE	4,096	3.192	0.004590
69	EUROPEAN JOURNAL OF PAIN	7,263	3.188	0.011070
70	Journal of Neurogastroenterology and Motility	1,407	3.179	0.002950
71	Behavioral Sleep Medicine	1,285	3.171	0.002350
72	JOURNAL OF NEURO-ONCOLOGY	11,487	3.129	0.016820
73	BRAIN TOPOGRAPHY	2,629	3.104	0.004920
74	JOURNAL OF THE INTERNATIONAL NEUROPSYCHOLOGICAL SOCIETY	6,773	3.098	0.007380
75	Nature and Science of Sleep	520	3.054	0.001290
76	NEUROGENETICS	1,268	3.017	0.002320
77	JOURNAL OF NEUROSURGERY-SPINE	7,809	2.998	0.012310
78	JOURNAL OF NEUROSURGICAL ANESTHESIOLOGY	1,495	2.957	0.001710
79	Pain Physician	4,377	2.942	0.007300
80	JOURNAL OF NEURAL TRANSMISSION	6,900	2.903	0.008030
80	SPINE	47,839	2.903	0.033120
82	CLINICAL JOURNAL OF PAIN	6,940	2.893	0.009670
83	Neurosurgical Focus	7,349	2.891	0.010090
84	Amyotrophic Lateral Sclerosis and Frontotemporal Degeneration	3,561	2.883	0.006060
85	Neurocritical Care	4,070	2.857	0.006910
86	ACTA NEUROLOGICA SCANDINAVICA	6,767	2.852	0.007200

Rank	Full Journal Title	Total Cites	Journal Impact Factor	Eigenfactor Score
87	NEUROLOGIC CLINICS	2,233	2.802	0.003290
88	Clinical Neuroradiology	798	2.800	0.002250
89	Neurodegenerative Diseases	1,560	2.798	0.002450
90	Journal of Clinical Neurology	1,268	2.796	0.002740
91	Current Pain and Headache Reports	2,158	2.767	0.003690
92	SEIZURE-EUROPEAN JOURNAL OF EPILEPSY	5,557	2.765	0.010290
93	JOURNAL OF GERIATRIC PSYCHIATRY AND NEUROLOGY	1,632	2.747	0.001840
94	Multiple Sclerosis and Related Disorders	1,621	2.725	0.005690
95	NEUROEPIDEMIOLOGY	3,266	2.689	0.004980
96	CEREBROVASCULAR DISEASES	5,517	2.681	0.007400
97	JOURNAL OF HEAD TRAUMA REHABILITATION	4,388	2.667	0.005850
98	NEUROMODULATION	2,109	2.663	0.004600
99	JOURNAL OF THE NEUROLOGICAL SCIENCES	17,679	2.651	0.023320
100	Frontiers in Neurology	6,274	2.635	0.019550
101	Journal of Neurologic Physical Therapy	1,022	2.614	0.001550
102	NEUROMUSCULAR DISORDERS	5,164	2.612	0.008560
103	CHILD NEUROPSYCHOLOGY	2,296	2.577	0.002780
104	NEUROSURGERY CLINICS OF NORTH AMERICA	1,637	2.553	0.002420
105	NEUROSURGICAL REVIEW	2,434	2.532	0.002960
106	EUROPEAN SPINE JOURNAL	16,408	2.513	0.021220
107	JOURNAL OF NEURO-OPHTHALMOLOGY	1,748	2.509	0.002520
108	NEURORADIOLOGY	5,656	2.504	0.007020
109	EUROPEAN JOURNAL OF PAEDIATRIC NEUROLOGY	2,764	2.496	0.005830

Rank	Full Journal Title	Total Cites	Journal Impact Factor	Eigenfactor Score
110	Pain Practice	2,422	2.486	0.004520
111	CLINICAL AUTONOMIC RESEARCH	1,761	2.485	0.001950
112	NEUROLOGICAL SCIENCES	5,637	2.484	0.009990
113	JOURNAL OF NEURORADIOLOGY	985	2.467	0.001440
114	JOURNAL OF THE PERIPHERAL NERVOUS SYSTEM	1,600	2.441	0.002130
115	MUSCLE & NERVE	12,279	2.393	0.014620
116	ALZHEIMER DISEASE & ASSOCIATED DISORDERS	3,166	2.378	0.003210
116	EPILEPSY & BEHAVIOR	10,335	2.378	0.017530
118	PEDIATRIC NEUROLOGY	5,398	2.326	0.009570
118	Sleep and Breathing	3,128	2.326	0.006070
120	CANADIAN JOURNAL OF NEUROLOGICAL SCIENCES	2,908	2.286	0.003590
121	PSYCHIATRY RESEARCH-NEUROIMAGING	5,503	2.270	0.008330
122	HUMAN PSYCHOPHARMACOLOGY-CLINICAL AND EXPERIMENTAL	2,149	2.265	0.002320
123	DEMENTIA AND GERIATRIC COGNITIVE DISORDERS	4,583	2.260	0.003830
124	Journal of Pain Research	2,171	2.236	0.006190
125	BMC Neurology	5,121	2.233	0.012460
126	Neuropsychiatric Disease and Treatment	5,337	2.228	0.012260
127	EPILEPSY RESEARCH	6,815	2.178	0.009800
128	REVUE NEUROLOGIQUE	1,943	2.177	0.002500
129	Journal of Neurosurgery-Pediatrics	4,167	2.170	0.007920
130	NEUROPHYSIOLOGIE CLINIQUE-CLINICAL NEUROPHYSIOLOGY	1,230	2.167	0.001380
131	NEUROPATHOLOGY	1,783	2.161	0.002720

Rank	Full Journal Title	Total Cites	Journal Impact Factor	Eigenfactor Score
132	JOURNAL OF CHILD NEUROLOGY	6,113	2.092	0.008940
133	JOURNAL OF NEUROIMAGING	2,081	2.080	0.004270
134	OTOLOGY & NEUROTOLOGY	8,094	2.063	0.011170
135	EPILEPTIC DISORDERS	1,305	2.052	0.002400
136	Parkinsons Disease	1,205	2.051	0.002290
137	NEUROLOGIA	1,077	2.038	0.001930
138	CLINICAL NEUROPSYCHOLOGIST	3,186	2.006	0.003220
139	JOURNAL OF CLINICAL AND EXPERIMENTAL NEUROPSYCHOLOGY	5,419	1.994	0.004060
140	NEUROLOGICAL RESEARCH	3,894	1.983	0.003940
141	JOURNAL OF NEUROPSYCHIATRY AND CLINICAL NEUROSCIENCES	3,615	1.971	0.002540
142	BEHAVIOURAL NEUROLOGY	1,340	1.908	0.002430
143	SPINAL CORD	5,874	1.898	0.005740
144	Journal of Neurosurgical Sciences	833	1.883	0.001270
145	JOURNAL OF NERVOUS AND MENTAL DISEASE	8,182	1.859	0.007030
146	ACTA NEUROCHIRURGICA	9,486	1.834	0.009160
147	CLINICAL EEG AND NEUROSCIENCE	1,018	1.822	0.001510
148	CURRENT NEUROVASCULAR RESEARCH	1,044	1.811	0.001370
149	BRAIN & DEVELOPMENT	3,930	1.756	0.004940
150	Clinical Spine Surgery	848	1.726	0.003160
151	World Neurosurgery	10,159	1.723	0.023420
152	JOURNAL OF SPINAL CORD MEDICINE	2,488	1.711	0.003110
153	Pain Research & Management	1,517	1.701	0.002530

Rank	Full Journal Title	Total Cites	Journal Impact Factor	Eigenfactor Score
154	JOURNAL OF CLINICAL NEUROPHYSIOLOGY	3,076	1.673	0.003540
155	CLINICAL NEUROLOGY AND NEUROSURGERY	5,855	1.672	0.010530
156	APHASIOLOGY	2,862	1.669	0.001970
157	NEUROPEDIATRICS	1,674	1.654	0.002050
158	NEUROLOGIA MEDICO-CHIRURGICA	3,018	1.651	0.002670
159	ACTA NEUROLOGICA BELGICA	991	1.612	0.001670
160	JOURNAL OF CLINICAL NEUROSCIENCE	8,027	1.593	0.013450
161	Korean Journal of Pain	512	1.563	0.000920
162	Applied Neuropsychology-Adult	426	1.548	0.001290
163	Applied Neuropsychology-Child	256	1.528	0.000830
164	Seminars in Pediatric Neurology	1,143	1.506	0.001320
165	BRITISH JOURNAL OF NEUROSURGERY	3,247	1.481	0.003140
166	SEMINARS IN NEUROLOGY	1,761	1.473	0.002650
167	Operative Neurosurgery	632	1.470	0.001450
168	American Journal of Alzheimers Disease and Other Dementias	2,062	1.464	0.002860
169	INTERVENTIONAL NEURORADIOLOGY	1,340	1.450	0.002280
170	Cognitive and Behavioral Neurology	766	1.396	0.000790
171	CHILDS NERVOUS SYSTEM	5,817	1.327	0.006110
172	CLINICAL NEUROPHARMACOLOGY	2,110	1.272	0.001550
173	SCHMERZ	746	1.267	0.000900
174	Developmental Neurorehabilitation	835	1.239	0.001590
175	EUROPEAN NEUROLOGY	3,068	1.235	0.003160
176	Journal of Neurological Surgery Part B-Skull Base	669	1.216	0.001690

Rank	Full Journal Title	Total Cites	Journal Impact Factor	Eigenfactor Score
177	NEUROREHABILITATION	2,546	1.197	0.003990
178	Journal of Korean Neurosurgical Society	1,991	1.187	0.002780
179	NEUROCASE	1,181	1.108	0.001620
180	JOURNAL OF NEUROSCIENCE NURSING	1,071	1.096	0.000970
181	Journal of Neurological Surgery Part A-Central European Neurosurgery	510	1.060	0.001360
182	Neurologia i Neurochirurgia Polska	835	1.006	0.001310
183	Brain Impairment	357	0.958	0.000430
184	NEUROCHIRURGIE	849	0.948	0.000840
185	CLINICAL NEUROPATHOLOGY	917	0.947	0.000860
186	Annals of Indian Academy of Neurology	1,013	0.898	0.001970
187	Turkish Neurosurgery	1,271	0.896	0.001870
188	Neurosciences	504	0.892	0.000760
189	Noropsikiyatri Arsivi-Archives of Neuropsychiatry	377	0.856	0.000740
190	NERVENARZT	1,603	0.829	0.001420
191	NEUROLOGIST	874	0.802	0.000460
192	PEDIATRIC NEUROSURGERY	2,001	0.783	0.000720
193	Sleep and Biological Rhythms	600	0.752	0.000830
194	FORTSCHRITTE DER NEUROLOGIE PSYCHIATRIE	534	0.635	0.000460
195	REVISTA DE NEUROLOGIA	1,755	0.485	0.001080
196	KLINISCHE NEUROPHYSIOLOGIE	40	0.325	0.000030
197	Zeitschrift fur Neuropsychologie	78	0.233	0.000090
198	Neurology Asia	215	0.218	0.000310
199	Ideggyogyaszati Szemle-Clinical Neuroscience	144	0.113	0.000150

frontiers in Neurology

Druckexemplar der Publikation

ORIGINAL RESEARCH
published: 05 May 2020
doi: 10.3389/fneur.2020.00381

The Effect of Scan Length on the Assessment of BOLD Delay in Ischemic Stroke

*Ayse Ceren Tanrıtanır [1], Kersten Villringer [1], Ivana Galinovic [1], Ulrike Grittner [2,3], Evgeniya Kirilina [4,5], Jochen B. Fiebach [1], Arno Villringer [6,7] and Ahmed A. Khalil [1,3,6,7]**

[1] Center for Stroke Research, Charité - Universitätsmedizin Berlin, Berlin, Germany, [2] Institute of Biometry and Clinical Epidemiology, Charité – Universitätsmedizin Berlin, Berlin, Germany, [3] Berlin Institute of Health (BIH), Berlin, Germany, [4] Department of Neurophysics, Max Planck Institute for Human Cognitive and Brain Sciences, Leipzig, Germany, [5] Center for Cognitive Neuroscience Berlin, Free University, Berlin, Germany, [6] Berlin School of Mind and Brain, Humboldt Universität zu Berlin, Berlin, Germany„ [7] Department of Neurology, Max Planck Institute for Human Cognitive and Brain Sciences, Leipzig, Germany

OPEN ACCESS

Edited by:
Peter Sörös,
University of Oldenburg, Germany

Reviewed by:
Bradley J. MacIntosh,
Sunnybrook Research Institute (SRI), Canada
Seena Dehkharghani,
New York University, United States

**Correspondence:*
Ahmed A. Khalil
ahmed-abdelrahim.khalil@charite.de

Specialty section:
This article was submitted to Applied Neuroimaging, a section of the journal Frontiers in Neurology

Received: 05 December 2019
Accepted: 15 April 2020
Published: 05 May 2020

Citation:
Tanrıtanır AC, Villringer K, Galinovic I, Grittner U, Kirilina E, Fiebach JB, Villringer A and Khalil AA (2020) The Effect of Scan Length on the Assessment of BOLD Delay in Ischemic Stroke. Front. Neurol. 11:381. doi: 10.3389/fneur.2020.00381

Objectives: To evaluate the impact of resting-state functional MRI scan length on the diagnostic accuracy, image quality and lesion volume estimation of BOLD delay maps used for brain perfusion assessment in acute ischemic stroke.

Methods: Sixty-three acute ischemic stroke patients received a 340 s resting-state functional MRI within 24 h of stroke symptom onset. BOLD delay maps were calculated from the full scan and four shortened versions (68 s, 136 s, 204 s, 272 s). The BOLD delay lesions on these maps were compared in terms of spatial overlap and volumetric agreement with the lesions derived from the full scans and with time-to-maximum (Tmax) lesions derived from DSC-MRI in a subset of patients (n = 10). In addition, the interpretability and quality of these maps were compared across different scan lengths using mixed models.

Results: Shortened BOLD delay scans showed a small volumetric bias (ranging from 0.05 to 5.3 mL; between a 0.13% volumetric underestimation and a 7.7% overestimation relative to the mean of the volumes, depending on scan length) compared to the full scan. Decreased scan length was associated with decreased spatial overlap with both the BOLD delay lesions derived from the full scans and with Tmax lesions. Only the two shortest scan lengths (68 and 136 s) were associated with substantially decreased interpretability, decreased structure clarity, and increased noisiness of BOLD delay maps.

Conclusions: BOLD delay maps derived from resting-state fMRI scans lasting 272 and 204 s provide sufficient diagnostic quality and adequate assessment of perfusion lesion volumes. Such shortened scans may be helpful in situations where quick clinical decisions need to be made.

Keywords: perfusion, acute stroke, BOLD delay, scan length, MRI

INTRODUCTION

The assessment of brain perfusion in acute ischemic stroke can be used to guide clinical decision-making, particularly when considering the use of intravenous thrombolysis or mechanical thrombectomy in patients otherwise ineligible for these treatments (1–3). Dynamic susceptibility contrast MRI (DSC-MRI) is most commonly used for this purpose in routine clinical practice.

However, it requires the use of exogenous contrast agents, which have potentially severe side effects (4). Even in people with normal kidney function, the gadolinium-based contrast agents used for DSC-MRI accumulate in the brain with repeated administration (5, 6), which has led the European Medicines Agency to recommend restricting their use (7).

As part of the ongoing search for alternative perfusion imaging methods, many studies have recently shown that the temporal properties of the blood-oxygenation-level-dependent (BOLD) signal reflect aspects of perfusion. This is because the BOLD signal, while usually used to probe the hemodynamic response to neural activity, reflects an amalgam of different physiological processes. These include fluctuations originating from outside the brain that travel through the vasculature in a manner closely resembling blood flow (8–11). These non-neuronal oscillations, referred to as systemic low-frequency oscillations (sLFOs), exist in the low-frequency range of the signal (0.01–0.15 Hz). Studies have shown changes in the amplitude, frequency, and phase of sLFOs in areas of low blood flow (12–15). Currently, one of the most well-studied temporal properties of the BOLD signal in relation to perfusion is BOLD delay (also known as hemodynamic lag)–the delay in arrival of sLFOs to a certain voxel compared to a reference region (14).

Evidence for the relationship between BOLD delay and perfusion comes from several sources. Firstly, regions of BOLD delay have been detected in cerebrovascular disorders including stroke (14, 16–21), transient ischemic attack (22), and Moyamoya disease (23). Such regions are also observed in other conditions associated with more subtle changes in cerebral perfusion such as Alzheimer's disease (24), epilepsy (25), and sickle cell disease (26). Secondly, direct comparisons between perfusion modalities have shown that BOLD delay correlates with measures of perfusion derived from DSC-MRI (14, 16, 18–21, 27) and arterial spin labeling (17, 22, 23). In addition, we have recently shown that increased BOLD delay in acute stroke due to large vessel occlusion is reversible following vessel recanalization, and that this reversibility mirrors reperfusion detected using DSC-MRI (19). Thirdly, manipulation of the circulatory system through respiratory challenges affects sLFOs in a manner consistent with changes in cerebrovascular reactivity (28–34). Finally, the physiological basis for BOLD delay seems to lie in axial variations in the concentration of deoxyhemoglobin within arteries and veins caused by vasomotion or changes in oxygen saturation (35). These variations act as a "virtual tracer"—a contrast agent intrinsic to the blood (35).

All this evidence suggests that the use of BOLD delay for assessing perfusion is a promising alternative to DSC-MRI. However, the clinical applicability of BOLD delay is still limited due to its relatively long acquisition time, which particularly hampers its use in clinical situations where decisions have to be made extremely quickly, such as in acute stroke. Studies utilizing BOLD delay for brain perfusion assessment have varied widely in scan length, between 3.5 and 30 min (see **Table 1** for an overview), markedly longer than typical DSC-MRI scans (~2 min). In this study, we evaluated the impact of scan length on the diagnostic accuracy, image quality and lesion volume estimation of BOLD delay maps used for brain perfusion assessment in acute ischemic stroke.

TABLE 1 | Overview of resting-state functional MRI scan lengths used in previous studies on BOLD delay for the assessment of brain perfusion.

Study	Investigated population	Scan length (min:s)
Lv et al. (14)	Acute stroke	5:50
Amemiya et al. (16)	Acute stroke and chronic hypoperfusion	10:00
Qian et al. (36)	Acute stroke	10:00
Christen et al. (23)	Moyamoya disease	3:36
Cologner et al. (26)	Sickle cell disease	6:00
Siegel et al. (17)	Subacute stroke	30:00[a]
Qian et al. (37)	Healthy individuals	6:40
Khalil et al. (18)	Acute stroke	5:50
Ni et al. (20)	Subacute stroke	8:00
Wu et al. (38)	Chronic hypoperfusion and moyamoya disease	5:00[b]
Tong et al. (27)	Healthy individuals	6:00
Chen et al. (21)	Acute stroke	8:00
Yang et al. (39)	Healthy individuals	10:00
Lv et al. (22)	Transient ischemic attack	8:00
Yan et al. (24)	Alzheimer's disease, mild cognitive impairment, and healthy individuals	6:40
Khalil et al. (19)	Acute stroke	5:50
Zhao et al. (40)	Chronic stroke	6:15
Nishida et al. (32)	Chronic hypoperfusion and moyamoya disease	7:20
Jahanian et al. (41)	Moyamoya disease and healthy individuals	4:00 to 6:00

[a] *Minimum of 5 min of resting-state functional MRI data after motion scrubbing required.*
[b] *Total resting-state functional MRI data acquired was 20 min, but data was divided into pre- and post-acetazolamide administration (5 min each) for processing.*

MATERIALS AND METHODS

Study Design

Patients with a confirmed clinical and radiological diagnosis of ischemic stroke who received a resting-state functional MRI scan together with a standard stroke protocol were recruited as part of the Longitudinal MRI Examinations of Patients With Brain Ischemia and Blood-Brain Barrier Permeability [LOBI-BBB] study clinicaltrials.gov NCT02077582 from June 2016 to December 2017. The LOBI-BBB study is a single-center, prospective cohort study of patients with acute ischemic stroke. A subset of patients received a follow-up (day 1) scan within 24 h of the first scan session (day 0 scan). This study was approved by the local institutional review board (EA1/200/13) and only patients who gave written informed consent were included. No exclusion criteria based on head motion were used, because we aimed at achieving a representative clinical population in our sample.

Imaging Protocol

A standard stroke MRI protocol was performed on a Siemens (Erlangen, Germany) Tim Trio 3 Tesla MRI scanner. The imaging protocol included a $T2^*$-weighted image

(TR/TE=669/20 ms, matrix = 320 × 320, field of view = 220 mm, slice thickness = 5 mm, acquisition time = 1 min 21 s), a diffusion-weighted image (TR/TE = 8900/93 ms, matrix = 192 × 192, field of view = 229 mm, slice thickness = 2.5 mm, acquisition time = 2 min 21 s), a FLAIR image (TR/TE = 8000/96 ms, matrix = 232 × 256, field of view = 199* 220 mm, slice thickness = 5 mm, acquisition time = 1 min 21 s) and a time-of-flight MR angiography (TR/TE = 21/3.4 ms, matrix = 218 × 384, field of view = 162 × 199 mm, slice thickness = 0.5 mm, acquisition time = 3 min 2 s). In addition, a resting-state functional MRI was performed using a multiband EPI scan (University of Minnesota sequence cmrr_mbep2d_bold R008) (42, 43): [850 (resting state) time points, TR/TE = 400/30 ms, flip angle 43°, matrix = 64 × 64, 192 × 192 mm field of view (FOV), multiband factor = 6, thirty 4.0 mm thick slices, acquisition time: 340 s]. During the scan, patients were requested to relax, lie still, and close their eyes. In a subset of patients, DSC-MRI data were acquired following the injection of a bolus of 5 mL Gadovist 1 mol/L and a saline flush at a flow rate of 5 mL/s with the following scanning parameters: TR/TE = 1390/29 ms, flip angle = 60, matrix = 128 × 128, 21 slices, slice thickness = 5 mm, acquisition time =1 min 58 s.

Image Processing

Preprocessing

As a first step, the first 25 volumes (10 s) were removed from the full 340 s resting-state scan to allow for magnetization equilibrium. Then, four shortened sets of data of various lengths were produced from the resulting full 330 s resting state scan (68 s, 136 s, 204 s, 272 s), and are referred to in this paper as 0.2, 0.4, 0.6, 0.8 scan segments, respectively.

Preprocessing was performed on the resting-state data of differing lengths using FSL (https://fsl.fmrib.ox.ac.uk/fsl) and AFNI (https://afni.nimh.nih.gov/afni). This comprised volume realignment to the first volume, regression of the effect of three rigid body translations and three rotations, spatial smoothing with 6-mm Gaussian kernel, and band pass filtering (0.01–0.15 Hz). The mean framewise displacement across the scan segments (FD) was calculated (44) and rescaled (multiplied by 10) to increase the comparability of this variable with the rest of the coefficients in the mixed effects models. In addition, to assess the signal change related to head motion, DVARS was calculated, defined as the frame-to-frame root mean square change in voxel intensities averaged across the entire brain (44).

Time Shift Analysis

A template was used to extract the reference time series by averaging the BOLD signal across all voxels in the major venous sinuses. This template was created from the post-gadolinium high-resolution T1-weighted scans of eight subjects, as described in the Supplemental Material of (18). Briefly, segmented gray matter, white matter, and CSF tissue masks were combined and subtracted from the brain-extracted T1 image, leaving an image containing only the vessels. This was registered to MNI space, binarized, summed up across subjects, manually edited to remove voxels outside the major venous sinuses, and spatially smoothed.

The venous sinus was preferred over the whole brain signal because BOLD delay calculated using the venous sinus reference correlated more strongly with DSC-MRI-based perfusion maps in both chronic cerebrovascular disease (23) and acute stroke (18). The venous sinus reference also avoids the contamination of the BOLD delay assessment procedure by hypoperfused voxels because it extracts time courses from voxels outside the brain parenchyma.

BOLD delay maps were generated by assigning each voxel the value of the time shift that achieves maximum cross-correlation between the reference time series and the voxel's time series. For this purpose, we used *rapidtide*, which is a set of Python tools for finding time-lagged correlations (https://github.com/bbfrederick/rapidtide). Significance thresholds for the cross-correlation were set by *rapidtide* using a shuffling procedure (10,000 times) to calculate the distribution of null correlation values. To determine the offset associated with the highest correlation coefficient with the reference signal, we shifted the time course from −20 to +20 s. This long tracking range was necessary because delays in acute stroke patients have been shown to be very long (18, 19).

BOLD delay maps generated from the data of each scan segment were registered to an echo-planar imaging (EPI) template derived from a similar cohort of stroke patients (18, 19). A multi-stage registration procedure (rigid → affine → deformable) was applied using the *antsRegistrationSyn* script

TABLE 2 | Demographics and clinical characteristics of the study sample.

Variable	Whole sample	Patients with hypoperfusion
N	63	43
Age in years (median, IQR)	75 (65–79)	78 (65–83)
Sex (M/F)	39/24	23/20
Follow-up (*n*)	38	17
mRS (median, IQR)		
Admission	3 (2–4)	4 (3–4)
Discharge	2 (1–3)	3 (1–4)
NIHSS (median, IQR)		
Admission	4 (1–8)	7 (3–11)
Discharge	2 (0–3)	3 (1–5)
Previous stroke (*n*)	22	16
Time (in hours) from symptom onset to MRI (median, IQR)	9 (3–16)	8 (1–14)
Vessel occlusion on MRA (n)	26	24
Therapy (*n*)		
Thrombolysis	17	15
Mechanical thrombectomy	5	5
Stroke vascular territory (*n*)		
Anterior cerebral artery	1	0
Middle cerebral artery	29	19
Posterior cerebral artery	9	3
Multiple territories	24	21

MRS, Modified Rankin Scale; NIHSS, National Institutes of Health Stroke Scale.

from the ANTs software (http://stnava.github.io/ANTs/) (45). Lesions on the diffusion-weighted images (DWI) were manually delineated by a stroke researcher (A.C.T.) and checked by a senior stroke researcher and radiology resident (A.K.) The DWI and the delineated DWI lesions were registered to the template using ANTs. DWI lesions were masked during the registration process to improve registration (46). The results of all registrations were inspected visually for quality.

Quantitative Analysis

Patients with a visible perfusion lesion on their full-length BOLD delay maps (assessed by A.K., a stroke researcher and radiology resident with 7 years' experience with perfusion imaging in stroke) were eligible for quantitative analysis in this study. Perfusion lesions on the BOLD delay maps were automatically delineated using an in-house algorithm used in a previous study (19). This algorithm searches the vascular territory affected by the stroke (defined as the vascular territory where the acute DWI lesion is present) for areas of hypoperfusion on the BOLD delay maps. For this procedure, BOLD delay maps thresholded to >0 s, >2.3 s, and >4.6 s were analyzed separately, generating three perfusion lesion volume values for each dataset (one value per threshold). The potential influence of these thresholds on the outcomes of this study were accounted for in the models.

Spatial Comparison of BOLD Delay Lesions

The Dice similarity coefficient was used for spatially comparing perfusion lesions on BOLD delay maps from shorter scans with those from the full length scan. The Dice similarity coefficient is a statistic used for evaluating spatial overlap and ranges between +1 (perfect overlap) and 0 (no overlap) (47). The association between scan length and the Dice similarity coefficient value was investigated using a linear mixed model (two-level; random intercept), with head motion as a covariate (48).

Volumetric Comparison of BOLD Delay Lesions

BOLD delay lesion volumes were calculated and the following analyses were performed on them:

Bland-Altman analysis (49) was used for assessing the agreement between shorter scans and the full length scan on BOLD delay lesion volume.

A linear mixed effects model (two-level; random intercept and slope model) was used to investigate the association between scan length and BOLD delay lesion volume. Since the distribution of

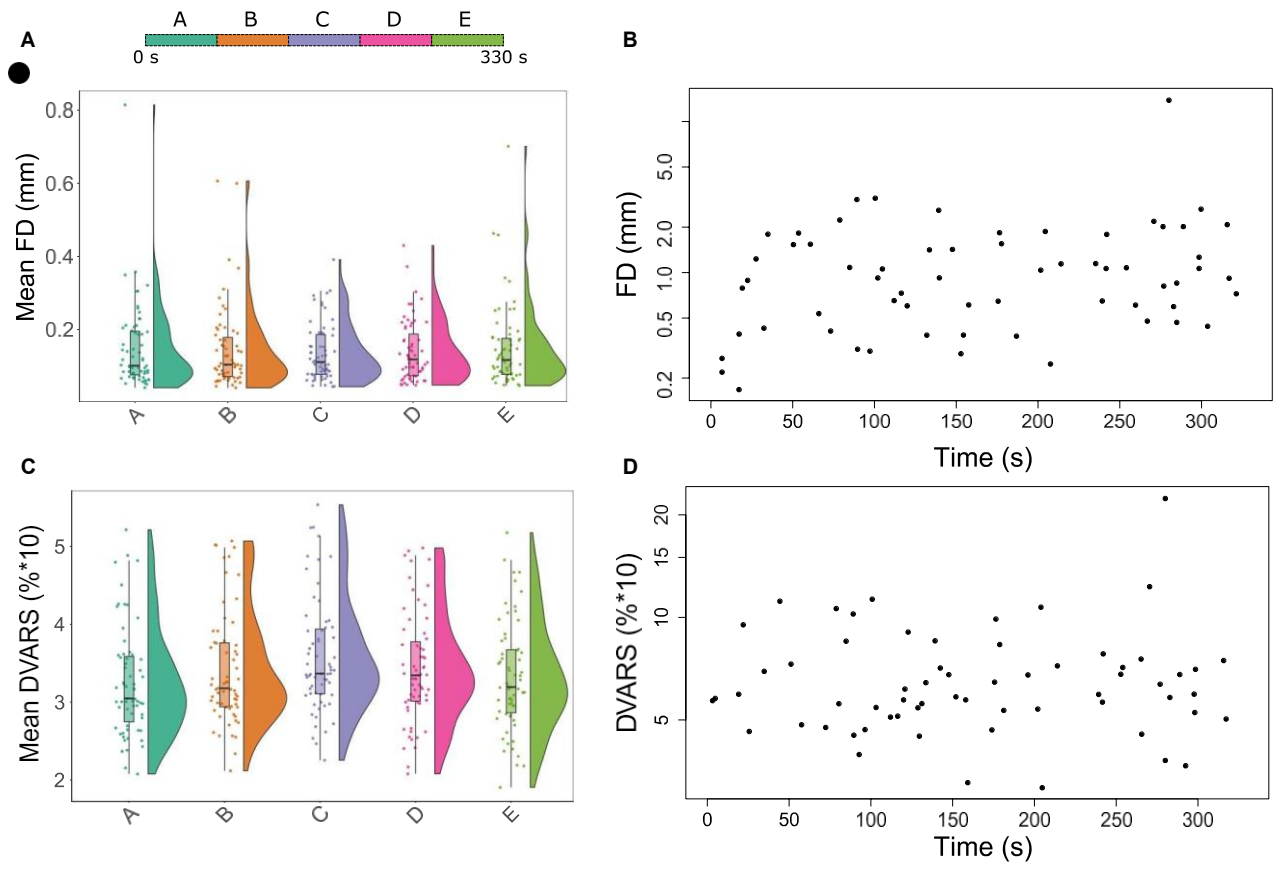

FIGURE 1 | Raincloud plots showing the distribution of mean head motion metrics (framewise displacement in (A) DVARS in (C) for each segment of the resting-state functional MRI scan. In Figures 1B,D, each point represents the maximum head motion value across the full scan (from one patient) measured using framewise displacement (B) and DVARS (D), plotted against time.

BOLD delay lesion volumes was skewed, the volumes were log-transformed for this analysis. The BOLD delay thresholds (0 s, 2.3 s, 4.6 s; ref = 0 s) and the scan sessions (day 0 or day 1; ref = day 0) were accounted for in this model.

Spatial and Volumetric Comparison of a Subsample of Patients With DSC-MRI Data

In a subsample of the patients eligible for quantitative analysis (n = 10), DSC-MRI data was acquired during the same scanning session after the rsfMRI scan. DSC-MRI data were analyzed using Stroketool version 2.8 (2011 Digital Image Solutions—HJ Wittsack) by selecting an arterial input function of 5–10 voxels in the middle cerebral artery contralateral to the acute infarction (50). Time-to-maximum (Tmax) maps were calculated using block-circulant singular value decomposition deconvolution of the concentration-time curve (51).

In this subsample, the Tmax maps were delineated using the same automated procedure described above for the BOLD delay maps, after applying a Tmax threshold of >6s (18, 52, 53). The Dice similarity coefficient was calculated between the perfusion lesions derived from each of the BOLD delay scans of different lengths and the Tmax maps. A Bland-Altman analysis was also performed to assess the agreement between Tmax perfusion lesion volumes and BOLD delay perfusion lesion volumes derived from the scans of different lengths.

Qualitative Analysis

Patients were included for qualitative analysis if they met the study's inclusion criteria, regardless of whether or not there was a visible perfusion lesion on their BOLD delay maps.

Two radiologists [K.V. [rater 1] and I.G. [rater 2]], both experienced in stroke perfusion imaging, visually assessed the BOLD delay maps of different scan lengths. The raters were blinded to all patient data and to the length of the scans from which the BOLD delay maps were generated, but had access to the DWI corresponding to each BOLD delay map. Prior to performing the readings, the raters were shown examples of the maps derived from an independent dataset (see **Supplementary Figure 2** for examples) and trained on how to fill in the data entry sheet.

Interpretability of Shortened BOLD Delay Maps

The raters assessed whether or not a perfusion lesion was visible on the BOLD delay maps, or if the BOLD delay map was uninterpretable. We calculated the agreement between the BOLD delay maps derived from each of the shortened scans and the BOLD delay maps derived from the full scan using unweighted Cohen's kappa. A binary logistic mixed model (48) (two level; random-intercept) was executed for comparing the interpretability of the BOLD delay maps (reference = "uninterpretable") derived from scans of different lengths while accounting for head motion and raters (ref = "rater 1").

Quality of BOLD Delay Maps

The raters assessed how noisy the BOLD delay maps were (on a scale of 1 to 3, with 3 indicating the highest level of noise) and how clear certain structures such as the ventricles were on the map (on a scale of 1 to 3, with 3 indicating the highest structure clarity). Examples of maps of various noisiness and structure clarity are shown in **Supplementary Figure 2**.

We used the quadratic-weighted Cohen's kappa (54) to assess the agreement between raters on the interpretability, noisiness, and structure clarity of the BOLD delay maps derived from each scan length.

Ordinal mixed models (55) were used to investigate the association between scan length and noise as well as structure clarity of the maps (two-level; random intercept models).

Note that in all statistical models used in this paper, subjects were level two units such that intra-individual correlation among the measures collected on a particular individual was taken into account and scan session identification (reference = "day 0") was included as a covariate in the models. All models in the qualitative analysis also accounted for the influence of the raters (reference ="rater 1").

Statistical Analysis

All statistical analyses were performed using *R* Statistical Software (56). The data and the code used for statistical analysis and data visualization in this study are publicly available at https://github.com/ahmedaak/BD_scan-shortening. Bland-Altman analysis was performed using the R package "blandr" (57), metrics of inter-rater agreement were calculated using the R package "irr" (58), linear mixed models using the "lmer" and "glmer" functions from the R package "lme4" (48), and ordinal mixed models using the "clmm" function from the R package "ordinal" (55). The distribution of continuous variables

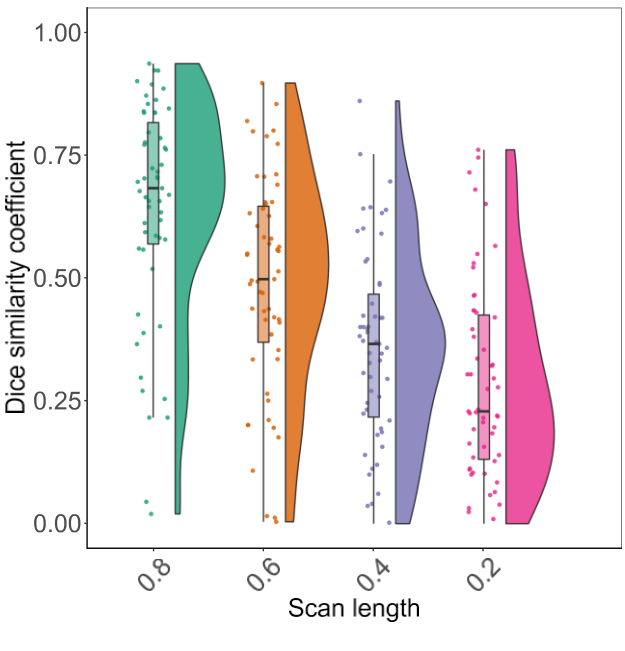

FIGURE 2 | Raincloud plots showing the distribution of Dice similarity coefficients (y axis) representing the degree of spatial overlap between BOLD delay lesions derived from resting-state functional MRI scans of different lengths (x axis) and the BOLD delay lesions derived from the full scan.

in different groups is visualized in this paper using raincloud plots, which combine dot plots, box plots, and violin plots (59). The distribution of categorical variables in different groups is visualized using spine plots (60).

RESULTS

Sixty-three patients who underwent an MRI scan within 24 h of stroke symptom onset were eligible for qualitative analysis. Forty-three of these patients had perfusion lesions on their BOLD delay maps and were selected for quantitative analysis. The characteristics of the two study groups for quantitative and qualitative analysis are presented separately in **Table 2**. The amount of head motion in each part of the rsfMRI scan is depicted for all patients in **Figure 1**.

The characteristics of the subsample who received a DSC-MRI scan are as follows: median age = 77.5 years (IQR = 63.5–80.3 years), median mRS at admission = 4 (IQR = 4–5), median mRS at discharge = 3 (IQR = 1–4), median NIHSS at admission = 11 (IQR = 7–16), median NIHSS at discharge = 4 (IQR = 2–8), median time from symptom onset to imaging = 1.5 h (IQR = 1–6.5 h). In this subsample, 7/10 patients were female, 3/10 had a follow-up MRI the next day, 4/10 had a previous stroke, 8/10 had a vessel occlusion on the TOF-MRA, 7/10 received intravenous thrombolysis, 4/10 received mechanical thrombectomy, 9/10 had an infarct in the MCA territory, and 1/10 had an infarct in the PCA territory. Data processing took a mean of 122 s (0.2 scan), 193 s (0.4 scan), 273 s (0.6 scan), 368 s (0.8 scan), and 411 s (full scan) per patient on an Intel® Xeon® X5570 CPU (2.93 GHz, 4 cores) with 64 GB of RAM. Note that a single thread was used for the processing.

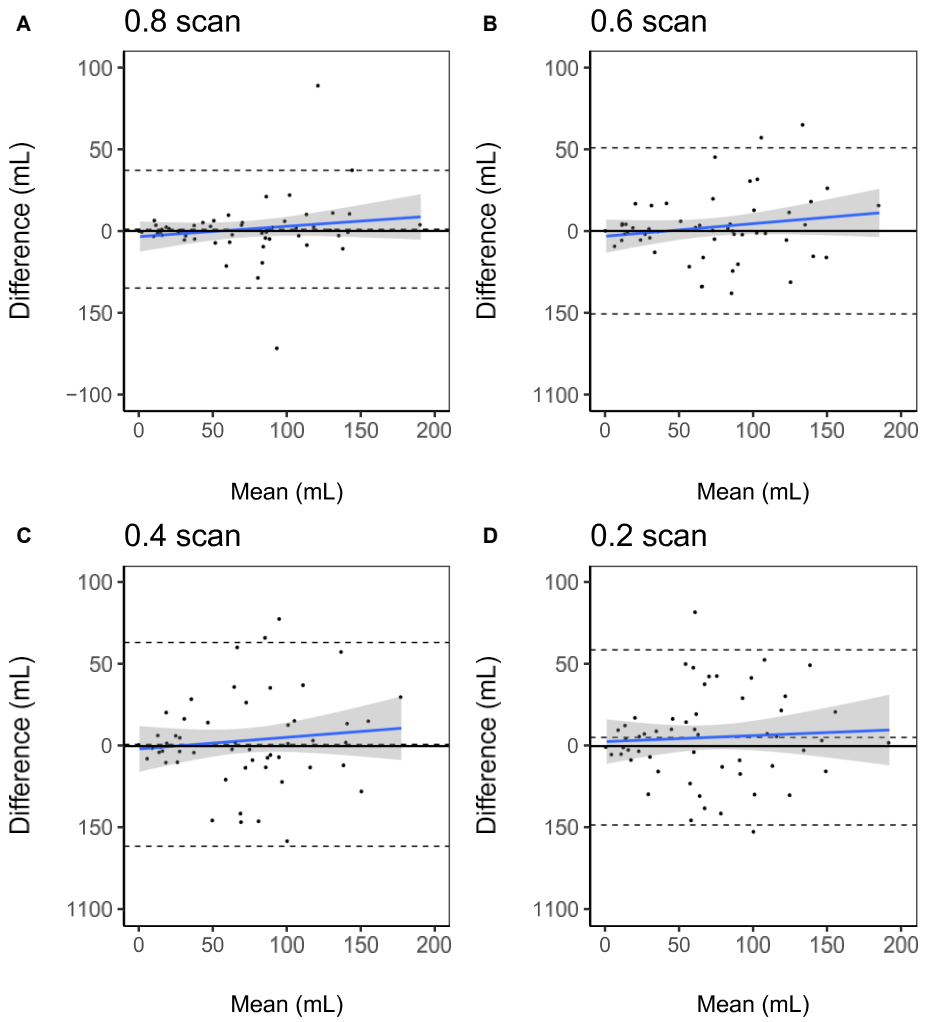

FIGURE 3 | Bland-Altman plots of volumetric agreement between BOLD delay lesion volumes derived from resting-state functional MRI scans of different lengths (A) 0.8 scan, (B) 0.6 scan, (C) 0.4 scan, (D) 0.2 scan and BOLD delay lesion volumes derived from the full scans. The upper and lower dashed lines represent the 95% limits of agreement and the middle dashed lines represent the bias (mean difference). The blue solid line and shaded gray region represent the regression lines and 95% confidence interval of the regression lines, respectively.

Quantitative Analysis

The DWIs and BOLD delay maps of all the patients in the quantitative analysis sample can be found here: https://doi.org/10.6084/m9.figshare.12022728.

Spatial Comparison of BOLD Delay Lesions

Figure 2 shows the distribution of spatial overlap metrics (Dice similarity coefficients) between BOLD delay lesions from each shortened scan and BOLD delay lesions from the full scan. The highest spatial overlap was between the 0.8 scan and the full scan (median = 0.68; IQR=0.56–0.81) and it decreased with decreasing scan length. The median Dice similarity coefficients between perfusion lesions from each BOLD delay scan length and Tmax perfusion lesions (for the subsample who also received DSC-MRI) were as follows: full scan =0.29 (IQR =0.02–0.33), 0.8 scan =0.26 (IQR =0.03–0.40), 0.6 scan =0.17 (IQR =0.03–0.39), 0.4 scan =0.1 (IQR =0.02–0.29), 0.2 scan =0.16 (IQR = 0.02–0.32).

The results of the linear mixed model of the association between scan length and spatial overlap showed that a 1% decrease in scan length was associated with a 0.006 reduction on average in the Dice coefficient between the BOLD delay lesions derived from the shortened scan and the full scan (beta = 0.006, SE =0.0004, t =13.6, $p < 0.0001$).

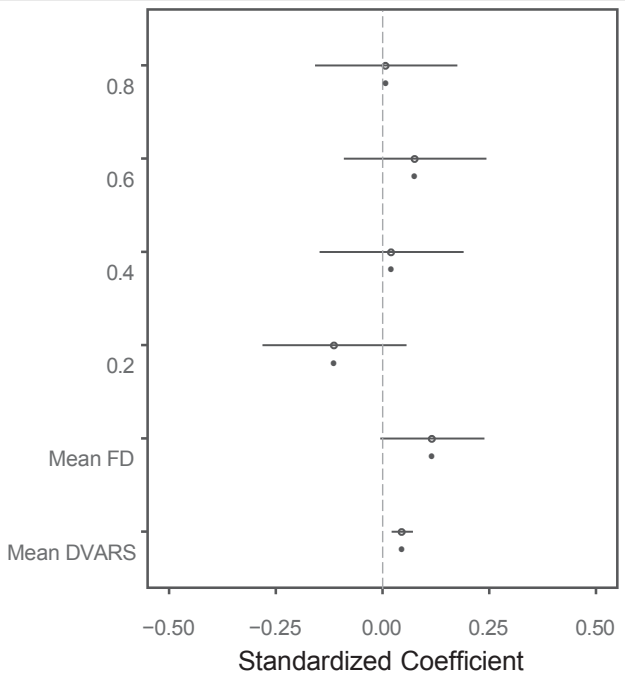

FIGURE 4 | Visualization of the results of the linear mixed model of the association between several predictors and BOLD delay lesion volumes. The points represent the standardized (beta) coefficients and the lines represent the 95% confidence intervals of the coefficients for each predictor. FD: framewise displacement. The scan lengths are shown as 0.8, 0.6, 0.4, and 0.2 with the full scan used as the reference category. This plot shows that the head motion metrics (mean FD and mean DVARS) are significantly associated with larger BOLD delay lesion volumes. There is no statistically significant difference between BOLD delay lesion volumes derived from the shorter resting-state functional MRI scans and the full scan. Note that only a subset of the predictors in this model are shown here—the numerical results of this linear mixed model, including the rest of the predictors, are shown in Supplementary Table 1.

Volumetric Comparison of BOLD Delay Lesions

The results of the Bland-Altman analysis are presented in **Figure 3** and the distribution of lesion volumes for each scan length is shown in **Supplementary Figure 1**. Compared to the BOLD delay lesion volumes derived from the full scan, the biases of the lesion volumes derived from the shortened scans were as follows: the 0.2 scan = 5.3 mL (a 7.7% overestimation relative to the mean of both scans, limits of agreement =−48.1–58.7 mL), 0.4 scan = 1.04 mL (a 4.5% overestimation relative to the mean of both methods, limits of agreement =−61.1–63.2), 0.6 scan = 0.05 mL (a 0.13% underestimation relative to the mean of both methods, limits of agreement =−50.6–50.7 mL), and 0.8 scan = 1.06 mL (a 1.4% overestimation relative to the mean of both methods, limits of agreement =−34.8–36.9 mL).

The results of the Bland-Altman analysis for the subsample who also received a DSC-MRI scan are shown in **Supplementary Figure 3**. Compared to the Tmax perfusion lesion volumes, the biases of the BOLD delay lesion volumes were as follows: the 0.2 scan = −14.5 mL (a 68.1% underestimation relative to the mean of both methods [BOLD delay and Tmax], limits of agreement = −80.6–51.5 mL), 0.4 scan = −8.2 mL (a 36.7% underestimation relative to the mean of both methods, limits of agreement = −68.0–51.7 mL), 0.6 scan = −18.3 mL (a 43.7% underestimation relative to the mean of both methods, limits of agreement = −80.2–43.5 mL), 0.8 scan = −17.2 (a 56.3% underestimation relative to the mean of both methods, limits of agreement = −65.7 to 31.3 mL), full scan = −12.9 mL (a 58.6% underestimation relative to the mean of both methods, limits of agreement = −58.6–32.6 mL).

The linear mixed model showed that there was no systematic impact of scan length on lesion volumes (**Figure 4** and **Supplementary Table 1**). Head motion measured using mean DVARS was associated with larger BOLD delay lesion volumes (beta =0.05, 95% CI =0.02–0.07, t =3.64, p =0.0003).

Qualitative Analysis

Diagnostic Accuracy

The interpretability of the BOLD delay maps derived from different scan lengths is shown in **Figure 5** for each of the raters. Agreement on map interpretability between BOLD delay maps derived from different scan lengths and those derived from the full scan are shown for each rater in **Supplementary Table 2**. The binary logistic mixed model revealed that scan lengths 0.2 (odds ratio = 0.21, 95% CI = 0.12–0.37, $p < 0.0001$) and 0.4 (odds ratio = 0.37, 95% CI = 0.21–0.64, p = 0.0004) were associated with decreased interpretability of the BOLD delay maps. Longer scans (0.8 and 0.6) showed no substantial association with interpretability of the BOLD delay maps (**Supplementary Table 3**).

Inter-Rater Agreement

Table 3 shows the inter-rater agreement on the interpretation, noisiness, and structure clarity of the BOLD delay maps derived

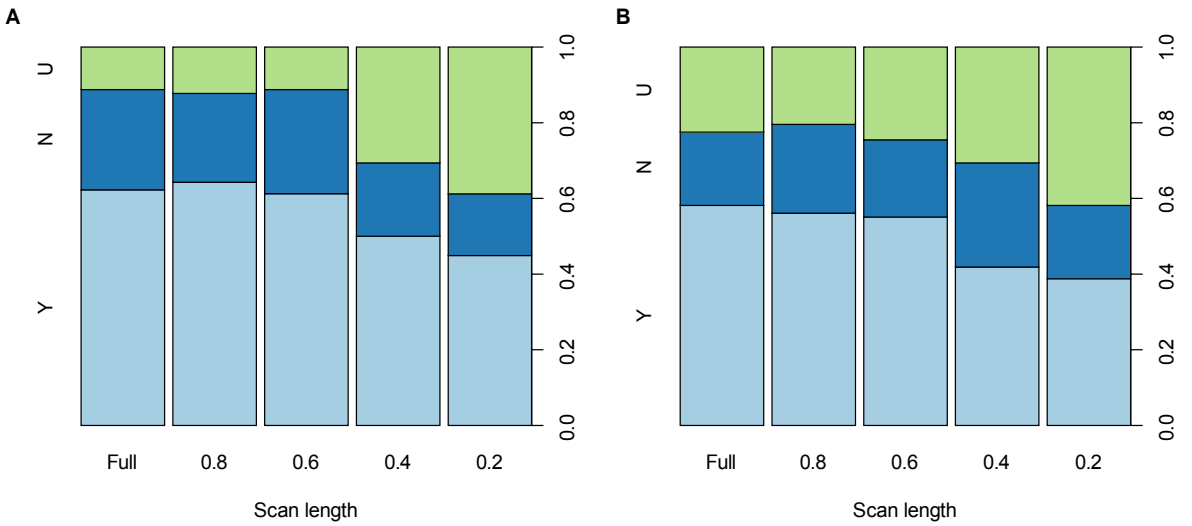

FIGURE 5 | Spine plots showing the distribution of the qualitative ratings of the BOLD delay maps derived from different resting-state functional MRI scan lengths made by rater 1 (A) and 2 (B) The maps were rated as either showing a perfusion lesion (Y, light blue), not showing a perfusion lesion (N, blue), or being uninterpretable (U, green). Statistically significant differences in interpretability are seen between the full scan and the 0.4 and 0.2 shortened scans. The quantitative results of the binary logistic mixed model investigating the effects of scan length on the interpretability of the BOLD delay maps are shown in Supplementary Table 3.

from different scan lengths. The raters' agreement on the interpretation of the BOLD delay maps was good across scan lengths (Cohen's kappa 0.64–0.82). Agreement on noisiness and structure clarity was markedly higher in the BOLD delay maps derived from the shorter scans than in those derived from the longer scans.

Quality of BOLD Delay Maps

The results of the qualitative assessment of scan noisiness and structure clarity by the two raters are shown in **Supplementary Figure 4**. The ordinal mixed models showed that scan lengths of 0.2 and 0.4, as well as head motion measured using mean framewise displacement and mean DVARS, were associated with more noise and less structure clarity on the BOLD delay maps (**Figure 6**). The quantitative results of the mixed models for noise and structure clarity are shown in **Supplementary Tables 4**, **5**, respectively.

DISCUSSION

In this study, the effects of scan length on the assessment of brain perfusion using BOLD delay maps in patients with ischemic stroke were systematically investigated. Our results show that scan length can be reduced from 5 min and 40 s to 3 min and 24 s without a significant loss of diagnostic accuracy and image quality of the BOLD delay maps.

A reduction of scan length by nearly two-and-a-half minutes is especially important in acute stroke, where patients are critically ill and decisions have to be made extremely quickly. The standard MRI protocol in our institution takes about 10 min (without perfusion imaging). Because time-to-treatment is a critical factor influencing stroke outcome, prolonging this by anything more than a few minutes is undesirable.

TABLE 3 | Inter-rater agreement (quadratic-weighted Cohen's kappa) on BOLD delay maps derived from different scan lengths.

Scan length	Interpretation[a]	Noise[b]	Structure clarity[b]
Full	0.64	0.22	0.40
0.8	0.71	0.29	0.15
0.6	0.82	0.25	0.26
0.4	0.75	0.67	0.40
0.2	0.67	0.72	0.48

[a] *Refers to whether the rater judged the map as showing aperfusion lesion, not showing a perfusion lesion, or being uninterpretable.*
[b] *Judged as high, medium or low.*

Our findings are overall in accordance with two previous studies. Lv et al. investigated the similarity between areas of BOLD signal delay and areas of hypoperfusion identified by DSC-MRI in acute stroke patients (61). The acquisition time was 5 min 50 s and the scan length was gradually decreased in increments of 10 volumes. They found that BOLD delay maps acquired in 3 min and 4 s provided qualitatively similar information to that of the full length scan in terms of overlap with the mean transit time (MTT; a parameter map derived from DSC-MRI) lesion of the subject. Christen et al., on the other hand, found that BOLD delay maps derived from resting-state functional MRI scans lasting 3 min and 36 s correlated highly with Tmax in Moyamoya patients (23). However, the impact of scan shortening on the diagnostic quality and clinical interpretability of BOLD delay maps was not systematically investigated in these studies.

In this study, agreement between raters on the evaluation of hypoperfusion presence at different scan lengths was good (weighted Cohen's kappa =0.64 to 0.82). Data on the inter-rater

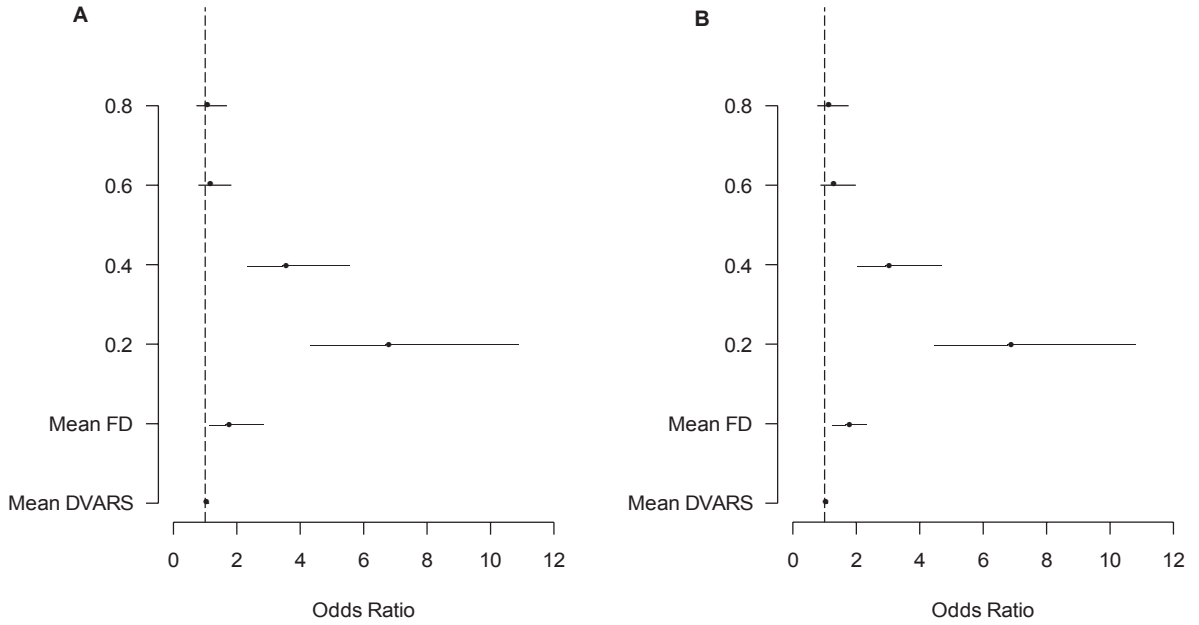

FIGURE 6 | Visualization of the results of the ordinal mixed models of the association between several predictors and BOLD delay map noisiness (A) and structure clarity (B). The points represent the odds ratios and the lines represent the 95% confidence intervals of the odds ratios for each predictor. The vertical dashed line represents an odds ratio of 1. FD, framewise displacement. The scan lengths are shown as 0.8, 0.6, 0.4, and 0.2 with the full scan used as the reference category. The plot shows that head motion (mean FD and mean DVARS) as well as the shortened 0.4 and 0.2 scans are associated with a significantly higher odds of more noise and less structure clarity than full scans. Note that only a subset of the predictors in this model are shown here—the numerical results of this ordinal mixed model, including the rest of the predictors, are shown in Supplementary Table 4 (noisiness) and 5 (structure clarity).

agreement of this relatively new perfusion imaging method has thus far been unavailable. In a study of 105 acute stroke patients, a similar level of inter-rater agreement on detecting perfusion deficits was found for DSC-MRI and ASL, with weighted Cohen's kappa values of 0.64 and 0.6, respectively (62). In our study, agreement on interpretability, structure clarity, and noisiness of the BOLD delay maps was higher for shorter scans than longer scans. This may be explained by the relative ease with which poor quality maps were judged by the raters. Overall, we found that the inter-rater agreement of this relatively new perfusion imaging method is similar to that observed when using more established perfusion imaging methods.

Several factors potentially interact with scan length to influence the diagnostic quality of BOLD delay maps. The temporal resolution of the resting-state functional MRI sequence is one such factor. Although the BOLD oscillations driving the calculation of BOLD delay are likely slow (<0.15 Hz), scanning with high temporal resolution, as done in this study using multiband EPI (42, 43), has the advantage of allowing high-frequency cardiac and respiratory activity to be filtered out of the data.

Head motion, on the other hand, causes undesired changes in the BOLD signal (44, 63) that adversely affect the cross-correlation underlying BOLD delay calculation. In a recent pilot study, we found that the intra-subject reproducibility of BOLD delay values in stroke patients was adversely influenced by head motion (64). In the current study, we therefore accounted for subject head motion in our analysis of the relationship between scan length and BOLD delay map quality and found that head motion significantly and adversely affected the level of noise, the structure clarity, and the volume of BOLD delay lesions, independent of scan length.

Considering that head motion is one of the main drawbacks hindering BOLD delay's use for brain perfusion assessment (14), exploring appropriate and reliable ways of reducing motion and its effects on the BOLD signal is crucial. Retrospective motion correction techniques such as scrubbing, which effectively removes volumes with high motion, have shown promise in functional connectivity studies (44). However, such techniques require that a sufficient amount of low-motion data remain after the removal of high-motion volumes (46). For this to be applicable, we need to know the minimum amount of data needed to generate adequate results. In functional connectivity studies, 10 to 15 min of data generally provide the best test-retest reliability (65). Our results suggest that much less data is required to provide diagnostically acceptable BOLD delay maps. With this knowledge, real-time motion monitoring approaches can allow us to continue scanning until a sufficient amount of low-motion data is acquired (66). This would reduce waste by reducing overscanning and, more importantly, allows scans to be tailored to the urgency of specific clinical situations.

Our study has a few limitations. We were unable to acquire DSC-MRI data in the entire sample in order to directly compare the shortened BOLD delay maps with a reference standard.

This was primarily due to the fact that we no longer routinely perform DSC-MRI at our stroke center due to the European Medicines Agency's recent recommendation to restrict the use of gadolinium-based contrast agents (7). However, the relationship between BOLD delay and perfusion measured using DSC-MRI has been established in several independent studies (14, 16, 18–21, 27). In this study, we chose to retrospectively break up longer scans into smaller parts, which is not the same as acquiring several scans of varying lengths. We chose this strategy for practical reasons, as acquiring several scans of different lengths would have greatly prolonged the scanning protocol and would have been infeasible in the context of acute stroke. However, this choice potentially limits how generalizable are results are to real-life situations where shortened scans are independently acquired. In addition, it should be kept in mind that several other potential factors may interact with scan length to influence BOLD delay map quality, including sequence parameters and field strength. Investigating the influence of these factors is beyond the scope of this study, and is currently the focus of ongoing work by our group (64). Finally, whether scan times longer than the full scan implemented in the current study (5 min 40 s) provide even better BOLD delay map quality is yet to be investigated. Such scans would not, however, be suitable in situations where urgent decision-making is required, such as acute stroke.

In conclusion, we show that BOLD delay maps derived from resting-state fMRI scans lasting 3 min 24 s provide sufficient diagnostic quality and adequate assessment of perfusion lesion volumes. This implies that scans can be shortened beyond currently usual scan times, which may be helpful for reducing the effect of patient motion or in situations where quick clinical decisions need to be made. Our results represent an important step toward implementing BOLD delay for contrast-agent-free assessment of brain perfusion in acute stroke patients in routine clinical practice.

DATA AVAILABILITY STATEMENT

The data and the code used for statistical analysis and data visualization in this study are publicly available at https://github.com/ahmedaak/BD_scan-shortening.

ETHICS STATEMENT

The studies involving human participants were reviewed and approved by Charité institutional review board EA1/200/13. The patients/participants provided their written informed consent to participate in this study.

AUTHOR CONTRIBUTIONS

AT, AK, JF, and AV: Conception or design of the work. JF, KV, IG, EK, and AK: Data collection. UG, IG, KV, AK, and AT: Data analysis and interpretation. AT and AK: Drafting the article. AT, KV, IG, UG, EK, JF, AV, and AK: Critical revision of the article and final approval of the version to be published.

ACKNOWLEDGMENTS

The authors thank the University of Minnesota Center for Magnetic Resonance Research for providing the multiband EPI sequence used in this study. Dr. Ahmed Khalil is a participant in the BIH-Charité Junior Clinician Scientist Program funded by the Charité –Universitätsmedizin Berlin and the Berlin Institute of Health.

SUPPLEMENTARY MATERIAL

The Supplementary Material for this article can be found online at: https://www.frontiersin.org/articles/10.3389/fneur.2020.00381/full#supplementary-material

REFERENCES

1. Fisher M, Albers GW. Advanced imaging to extend the therapeutic time window of acute ischemic stroke. *Ann Neurol.* (2013) 73:4–9. doi: 10.1002/ana.23744
2. Luby M, Warach SJ, Albers GW, Baron J-C, Cognard C, Dávalos A, et al. Identification of imaging selection patterns in acute ischemic stroke patients and the influence on treatment and clinical trial enrollment decision making. *Int J Stroke*. (2016) 11:180–90. doi: 10.1177/1747493015616634
3. Albers GW, Marks MP, Kemp S, Christensen S, Tsai JP, Ortega-Gutierrez S, et al. Thrombectomy for stroke at 6 to 16 hours with selection by perfusion imaging. *N Engl J Med.* (2018) 378:708–18. doi: 10.1056/NEJMoa1713973
4. Kuo PH, Kanal E, Abu-Alfa AK, Cowper SE. Gadolinium-based MR contrast agents and nephrogenic systemic fibrosis. *Radiology*. (2007) 242:647–9. doi: 10.1148/radiol.2423061640
5. McDonald RJ, McDonald JS, Kallmes DF, Jentoft ME, Murray DL, Thielen KR, et al. Intracranial Gadolinium Deposition after Contrast-enhanced MR Imaging. *Radiology*. (2015) 275:772–82. doi: 10.1148/radiol.15150025
6. Gulani V, Calamante F, Shellock FG, Kanal E, Reeder SB. Gadolinium deposition in the brain: summary of evidence and recommendations. *Lancet Neurol.* (2017) 16:564–70. doi: 10.1016/S1474-4422(17)30158-8
7. European Medicines Agency. *Gadolinium-Containing Contrast Agents*. (2018) Available Online at: https://www.ema.europa.eu/; https://www.ema.europa.eu/en/medicines/human/referrals/gadolinium-containing-contrast-agents [Accessed November 7, 2019].
8. Tong Y, Hocke LM, Licata SC, Frederick BD. Low-frequency oscillations measured in the periphery with near-infrared spectroscopy are strongly correlated with blood oxygen level-dependent functional magnetic resonance imaging signals. *J Biomed Opt.* (2012) 17:106004. doi: 10.1117/1.JBO.17.10.106004
9. Tong Y, Hocke LM, Lindsey KP, Erdogan SB, Vitaliano G, Caine CE, et al. Systemic low-frequency oscillations in BOLD signal vary with tissue type. *Front Neurosci.* (2016) 10:313. doi: 10.3389/fnins.2016.00313
10. Tong Y, Yao J. (fiona), Chen JJ, Frederick B, de B. The resting-state fMRI arterial signal predicts differential blood transit time through the brain. *J Cereb Blood Flow Metab*. (2018) 39:1148–60. doi: 10.1177/0271678X17753329
11. Tong Y, Hocke LM, Frederick BB. Low frequency systemic hemodynamic "noise" in resting state BOLD fMRI: characteristics, causes, implications,

mitigation strategies, and applications. *Front Neurosci.* (2019) 13:787. doi: 10.3389/fnins.2019.00787
12. Liu Y, D'Arceuil H, He J, Duggan M, Gonzalez G, Pryor J, et al. MRI of spontaneous fluctuations after acute cerebral ischemia in nonhuman primates. *J Magn Reson Imaging*. (2007) 26:1112–6. doi: 10.1002/jmri.21131
13. Qun-li Y, Zhang HY, Nie BB, Fang F, Jiao Y, Teng GJ. MRI assessment of amplitude of low-frequency fluctuation in rat brains with acute cerebral ischemic stroke. *Neurosci Lett.* (2012) 509:22–6. doi: 10.1016/j.neulet.2011.12.036
14. Lv Y, Margulies DS, Cameron Craddock R, Long X, Winter B, Gierhake D, et al. Identifying the perfusion deficit in acute stroke with resting-state functional magnetic resonance imaging. *Ann Neurol.* (2013) 73:136–9. doi: 10.1002/ana.23763
15. Tsai Y-H, Yuan R, Huang Y-C, Weng H-H, Yeh M-Y, Lin C-P, et al. Altered resting-state FMRI signals in acute stroke patients with ischemic penumbra. *PLoS ONE*. (2014) 9:e105117. doi: 10.1371/journal.pone.0105117
16. Amemiya S, Kunimatsu A, Saito N, Ohtomo K. Cerebral hemodynamic impairment: assessment with resting-state functional MR imaging. *Radiology*. (2014) 270:548–55. doi: 10.1148/radiol.13130982
17. Siegel JS, Snyder AZ, Ramsey L, Shulman GL, Corbetta M. The effects of hemodynamic lag on functional connectivity and behavior after stroke. *J Cereb Blood Flow Metab.* (2016) 36:2162–76. doi: 10.1177/0271678X15614846
18. Khalil AA, Ostwaldt AC, Nierhaus T, Ganeshan R, Audebert HJ, Villringer K, et al. Relationship between changes in the temporal dynamics of the blood-oxygen-level-dependent signal and hypoperfusion in acute ischemic stroke. *Stroke*. (2017) 48:925–31. doi: 10.1161/STROKEAHA.116.015566
19. Khalil AA, Villringer K, Filleböck V, Hu JY, Rocco A, Fiebach JB, et al. Non-invasive monitoring of longitudinal changes in cerebral hemodynamics in acute ischemic stroke using BOLD signal delay. *J Cereb Blood Flow Metab.* (2018) 40:23–34. doi: 10.1177/0271678X18803951
20. Ni L, Li J, Li W, Zhou F, Wang F, Schwarz CG, et al. The value of resting-state functional MRI in subacute ischemic stroke: comparison with dynamic susceptibility contrast-enhanced perfusion MRI. *Sci Rep.* (2017) 7:41586. doi: 10.1038/srep41586
21. Chen Q, Zhou J, Zhang H, Chen Y, Mao C, Chen X, et al. One-step analysis of brain perfusion and function for acute stroke patients after reperfusion: A resting-state fMRI study. *J. Magn. Reson. Imaging*. (2018) 50:221–9. doi: 10.1002/jmri.26571
22. Lv Y, Wei W, Song Y, Han Y, Zhou C, Zhou D, et al. Non-invasive evaluation of cerebral perfusion in patients with transient ischemic attack: an fMRI study. *J Neurol*. (2018) 266:157–64. doi: 10.1007/s00415-018-9113-3
23. Christen T, Jahanian H, Ni WW, Qiu D, Moseley ME, Zaharchuk G. Noncontrast mapping of arterial delay and functional connectivity using resting-state functional MRI: a study in Moyamoya patients. *J Magn Reson Imaging*. (2015) 41:424–30. doi: 10.1002/jmri.24558
24. Yan S, Qi Z, An Y, Zhang M, Qian T, Lu J. Detecting perfusion deficit in Alzheimer's disease and mild cognitive impairment patients by resting-state fMRI. *J Magn Reson Imaging*. (2018) 49:1099–104. doi: 10.1002/jmri.26283
25. Shah MN, Mitra A, Goyal MS, Snyder AZ, Zhang J, Shimony JS, et al. Resting state signal latency predicts laterality in pediatric medically refractory temporal lobe epilepsy. *Childs Nerv Syst.* (2018) 34:901–10. doi: 10.1007/s00381-018-3770-5
26. Coloigner J, Vu C, Bush A, Borzage M, Rajagopalan V, Lepore N, et al. BOLD delay times using group delay in sickle cell disease. In: Styner MA, and Angelini ED, editors. *SPIE Medical Imaging*. San Diego, CA: International Society for Optics and Photonics (2016). p. 97843M. doi: 10.1117/12.2217263
27. Tong Y, Lindsey KP, Hocke LM, Vitaliano G, Mintzopoulos D, Frederick BD. Perfusion information extracted from resting state functional magnetic resonance imaging. *J Cereb Blood Flow Metab.* (2017) 37:564–76. doi: 10.1177/0271678X16631755
28. Mandell DM, Han JS, Poublanc J, Crawley AP, Stainsby JA, Fisher JA, et al. Mapping cerebrovascular reactivity using blood oxygen level-dependent MRI in patients with arterial steno-occlusive disease: comparison with arterial spin labeling MRI. *Stroke*. (2008) 39:2021–8. doi: 10.1161/STROKEAHA.107.506709
29. Golestani AM, Wei LL, Chen JJ. Quantitative mapping of cerebrovascular reactivity using resting-state BOLD fMRI: validation in healthy adults. *Neuroimage*. (2016) 138:147–63. doi: 10.1016/j.neuroimage.2016.05.025
30. Smeeing DPJ, Hendrikse J, Petersen ET, Donahue MJ, de Vis JB. Arterial spin labeling and blood oxygen level-dependent MRI cerebrovascular reactivity in cerebrovascular disease: a systematic review and meta-analysis. *Cerebrovasc Dis.* (2016) 42:288–307. doi: 10.1159/000446081
31. Fierstra J, Van Niftrik C, Warnock G, Wegener S, Piccirelli M, Pangalu A, et al. Staging hemodynamic failure with blood oxygen-level-dependent functional magnetic resonance imaging cerebrovascular reactivity a comparison versus gold standard (15O-)H2O-positron emission tomography. *Stroke*. (2018) 49:621–9. doi: 10.1161/STROKEAHA.117.020010
32. Nishida S, Aso T, Takaya S, Takahashi Y, Kikuchi T, Funaki T, et al. Resting-state functional magnetic resonance imaging identifies cerebrovascular reactivity impairment in patients with arterial occlusive diseases: a pilot study. *Neurosurgery*. (2018). 85:680–8. doi: 10.1093/neuros/nyy434
33. Venkatraghavan L, Poublanc J, Han JS, Sobczyk O, Rozen C, Sam K, et al. Measurement of cerebrovascular reactivity as blood oxygen level-dependent magnetic resonance imaging signal response to a hypercapnic stimulus in mechanically ventilated patients. *J Stroke Cerebrovasc Dis.* (2018) 27:301–8. doi: 10.1016/j.jstrokecerebrovasdis.2017.08.035
34. Prokopiou PC, Pattinson KTS, Wise RG, Mitsis GD. Modeling of dynamic cerebrovascular reactivity to spontaneous and externally induced CO2 fluctuations in the human brain using BOLD-fMRI. *Neuroimage*. (2019) 186:533–48. doi: 10.1016/j.neuroimage.2018.10.084
35. Aso T, Urayama S, Fukuyama H, Murai T. Axial variation of deoxyhemoglobin density as a source of the low-frequency time lag structure in blood oxygenation level-dependent signals. *PLoS ONE*. (2019) 14:e0222787. doi: 10.1371/journal.pone.0222787
36. Qian T, Wang ZAPG. Measuring the timing information of blood flow in acute stroke with the background. *Proc. Intl. Soc. Mag. Reson. Med.* (2015) 23:2195.
37. Qian T, Zanchi D, Rodriguez C, Ackermann M, Giannakopoulos P, Haller S. Detecting perfusion pattern based on the background low-frequency fluctuation in resting-state functional MRI data and its influence on resting-state networks: an iterative post-processing approach. *Brain Connect.* (2017) 7:627–34. doi: 10.1089/brain.2017.0545
38. Wu J, Dehkharghani S, Nahab F, Allen J, Qiu D. The effects of acetazolamide on the evaluation of cerebral hemodynamics and functional connectivity using blood oxygen level-dependent MR imaging in patients with chronic steno-occlusive disease of the anterior circulation. *Am J Neuroradiol.* (2017) 38:139–45. doi: 10.3174/ajnr.A4973
39. Yang H-CS, Liang Z, Yao JF, Shen X, Frederick BD, Tong Y. Vascular effects of caffeine found in BOLD fMRI. *J Neurosci Res.* (2018) 97:456–66. doi: 10.1002/jnr.24360
40. Zhao Y, Lambon Ralph MA, Halai AD. Relating resting-state hemodynamic changes to the variable language profiles in post-stroke aphasia. *NeuroImage.* (2018) 20:611–9. doi: 10.1016/j.nicl.2018.08.022
41. Jahanian H, Christen T, Moseley ME, Zaharchuk G. Erroneous resting-state fMRI connectivity maps due to prolonged arterial arrival time and how to fix them. *Brain Connect.* (2018) 8:362–70. doi: 10.1089/brain.2018.0610
42. Feinberg DA, Moeller S, Smith SM, Auerbach E, Ramanna S, Matt F, et al. Multiplexed echo planar imaging for sub-second whole brain FMRI and fast diffusion imaging. *PLoS ONE.* (2010) 5:e15710. doi: 10.1371/journal.pone.0015710
43. Xu J, Moeller S, Auerbach EJ, Strupp J, Smith SM, Feinberg DA, et al. Evaluation of slice accelerations using multiband echo planar imaging at 3 T. *Neuroimage*. (2013) 83:991–1001. doi: 10.1016/j.neuroimage.2013.07.055
44. Power JD, Barnes KA, Snyder AZ, Schlaggar BL, Petersen SE. Spurious but systematic correlations in functional connectivity MRI networks arise from subject motion. *Neuroimage*. (2012) 59:2142–54. doi: 10.1016/j.neuroimage.2011.10.018
45. Tustison NJ, Avants BB. Explicit B-spline regularization in diffeomorphic image registration. *Front Neuroinform.* (2013) 7:39. doi: 10.3389/fninf.2013.00039
46. Siegel JS, Shulman GL, Corbetta M. Measuring functional connectivity in stroke: approaches and considerations. *J Cereb Blood Flow Metab.* (2017) 37:2665–78. doi: 10.1177/0271678X17709198
47. Dice LR. Measures of the amount of ecologic association between species. *Ecology*. (1945) 26:297–302. doi: 10.2307/1932409
48. Bates D, Mächler M, Bolker B, Walker S. Fitting linear mixed-effects models using lme4. *J Stat Softw.* (2014) 67:1–48. doi: 10.18637/jss.v067.i01

49. Martin Bland J, Altman D. Statistical methods for assessing agreement between two methods of clinical measurement. *Lancet*. (1986) 327:307–10. doi: 10.1016/S0140-6736(86)90837-8
50. Ebinger M, Brunecker P, Jungehülsing GJ, Malzahn U, Kunze C, Endres M, et al. Reliable perfusion maps in stroke MRI using arterial input functions derived from distal middle cerebral artery branches. *Stroke*. (2010) 41:95–101. doi: 10.1161/STROKEAHA.109.559807
51. Wu O, Østergaard L, Weisskoff RM, Benner T, Rosen BR, Sorensen AG. Tracer arrival timing-insensitive technique for estimating flow in MR perfusion-weighted imaging using singular value decomposition with a block-circulant deconvolution matrix. *Magn Reson Med*. (2003) 50:164–74. doi: 10.1002/mrm.10522
52. Olivot JM, Mlynash M, Thijs VN, Kemp S, Lansberg MG, Wechsler L, et al. Optimal tmax threshold for predicting penumbral tissue in acute stroke. *Stroke*. (2009) 40:469–75. doi: 10.1161/STROKEAHA.108.526954
53. Zaro-Weber O, Moeller-Hartmann W, Heiss WD, Sobesky J. Maps of time to maximum and time to peak for mismatch definition in clinical stroke studies validated with positron emission tomography. *Stroke*. (2010) 41:2817–21. doi: 10.1161/STROKEAHA.110.594432
54. Cohen J. A coefficient of agreement for nominal scales. *Educ Psychol Meas.* (1960) 20:37–46. doi: 10.1177/001316446002000104
55. Christensen RHB. *Regression Models for Ordinal Data*. R package version 2019. (2019) 4–25. Available online at: http://www.cran.r-project.org/package=ordinal/
56. R Core Team. (2013). *R: A Language and Environment for Statistical Computing*. Available Online at: http://www.R-project.org/. (accessed March 19, 2020).
57. Datta D. blandr: a bland-altman method comparison package for R. (2017) 10. doi: 10.5281/zenodo.824514
58. Gamer M, Lemon J, and Puspendra Singh IF. (2019). irr: various coefficients of interrater reliability and agreement. Available at: https://CRAN.R-project.org/package=irr. (accessed January 8, 2020).
59. Allen M, Poggiali D, Whitaker K, Marshall TR, Kievit RA. Raincloud plots: a multi-platform tool for robust data visualization. *Wellcome Open Res*. (2019) 4:63. doi: 10.12688/wellcomeopenres.15191.1
60. Meyer D, Zeileis A, Hornik K. Visualizing Contingency Tables. In: Chen C-H, Härdle W, and Unwin A, editors. *Handbook of Data Visualization*. Springer Berlin Heidelberg (2008). p. 589–616. doi: 10.1007/978-3-540-33037-0_23
61. Lv Y. *Application of Resting-State fMRI Methods to Acute Ischemic Stroke Dissertation*. (2013).
62. Bokkers RPH, Hernandez DA, Merino JG, Mirasol RV, Van Osch MJ, Hendrikse J, et al. Whole-brain arterial spin labeling perfusion MRI in patients with acute stroke. *Stroke*. (2012) 43:1290–4. doi: 10.1161/STROKEAHA.110.589234
63. Van Dijk KRA, Sabuncu MR, Buckner RL. The influence of head motion on intrinsic functional connectivity MRI. *Neuroimage*. (2012) 59:431–8. doi: 10.1016/j.neuroimage.2011.07.044
64. Khalil AA, Tanritanir AC, Grittner U, Villringer A, Fiebach J, Mekle R. Reproducibility of BOLD delay perfusion measurements in acute stroke patients. In: *Proceedings of the International Society for Magnetic Resonance in Medicine*. (2018). Available Online at: http://archive.ismrm.org/2018/4823.html [Accessed November 7, 2019].
65. Birn RM, Molloy EK, Patriat R, Parker T, Meier TB, Kirk GR, et al. The effect of scan length on the reliability of resting-state fMRI connectivity estimates. *Neuroimage*. (2013) 83:550–8. doi: 10.1016/j.neuroimage.2013.05.099
66. Dosenbach NUF, Koller JM, Earl EA, Miranda-Dominguez O, Klein RL, Van AN, et al. Real-time motion analytics during brain MRI improve data quality and reduce costs. *Neuroimage*. (2017) 161:80–93. doi: 10.1016/j.neuroimage.2017.08.025

Conflict of Interest: KV and JF were funded by the German Federal Ministry of Education and Research (01EO0801, 01EO01301). JF has received consulting, lecture, advisory board fees from BioClinica, Cerevast, Artemida, Brainomix. AK, KV, and JF were co-inventors of a patent application relating to a method for automated, user-independent delineation of perfusion lesions, used in this manuscript.

The remaining authors declare that the research was conducted in the absence of any commercial or financial relationships that could be construed as a potential conflict of interest.

Mein Lebenslauf wird aus datenschutzrechtlichen Gründen in der elektronischen Version meiner Arbeit nicht veröffentlicht.

Mein Lebenslauf wird aus datenschutzrechtlichen Gründen in der elektronischen Version meiner Arbeit nicht veröffentlicht.

Mein Lebenslauf wird aus datenschutzrechtlichen Gründen in der elektronischen Version meiner Arbeit nicht veröffentlicht.

Mein Lebenslauf wird aus datenschutzrechtlichen Gründen in der elektronischen Version meiner Arbeit nicht veröffentlicht.

Mein Lebenslauf wird aus datenschutzrechtlichen Gründen in der elektronischen Version meiner Arbeit nicht veröffentlicht.

Publikationsliste

Posters:

Ayse Ceren Tanritanir, Kersten Villringer , Ivana Galinovic , Ulrike Grittner , Evgeniya Kirilina , Jochen B. Fiebach, Arno Villringer , Ahmed A. Khalil, *The effect of scan length on the assessment of perfusion using BOLD delay in ischemic stroke*, 05/2019, 27. Annual Meeting International Society of Magnetic
Resonance in Medicine (ISMRM), Montreal, Canada

Ayse Ceren Tanritanir, Marta Benet Mora, Judith Garcia Aymerich, Jose Maria Anto, *Temporal evolution of COPD phenotypes: FEV1 as the predictor variable in short feature,* 06/2015, 22. Annual Meeting International Student Congress Of (bio)Medical Sciences (ISCOMS), Groningen, the Netherlands

Oral Presentations:

Ayse Ceren Tanritanir, Kersten Villringer , Ivana Galinovic , Ulrike Grittner , Evgeniya Kirilina , Jochen B. Fiebach, Arno Villringer , Ahmed A. Khalil, *The effect of scan length on the assessment of perfusion using BOLD delay in ischemic stroke*, 05/2018, 4. Annual Meeting European Stroke Congress (ESOC), Gotheborg, Sweden

Ayse Ceren Tanritanir, David S. Newburg, Subrata Chakrabarti, *Lactodifucotetraose, a human milk oligosaccharide, attenuates platelet function and inflammatory cytokine release*, 06/2016, 23. Annual Meeting International Student Congress Of (bio)Medical Sciences (ISCOMS), Groningen, the Netherlands

Ayse Ceren Tanritanir, David S. Newburg, Subrata Chakrabarti, *Lactodifucotetraose, a human milk oligosaccharide, attenuates platelet function and inflammatory cytokine release,* 09/2014, 25.Annual Meeting European Students' Congress (ESC), Berlin, Germany

*(Alle Posters und Powerpoint Präsentationen wurden von mir erstellt unter Hilfestellung der o.g. Mitautor*innen)*

Manuscripts:

Ayse Ceren Tanritanir, Kersten Villringer , Ivana Galinovic , Ulrike Grittner , Evgeniya Kirilina , Jochen B. Fiebach, Arno Villringer , Ahmed A. Khalil, *The effect of scan length on the assessment of perfusion using BOLD delay in ischemic stroke,* Frontiers Neurology

DOI: 10.3389/fneur.2020.00381 Impact Factor 3,5

Tomo Tarui, Neel Madan, Nabgha Farhat, Rie Kitano, Ayse Ceren Tanritanir, George Graham, Borjan Gagoski, Alexa Craig, Caitlin Rollins, Cynthia Ortinau, Vidya Iyer, Ellen Grant, *Disorganized sulcal pattern in fetal brains with agenesis of corpus callosum,* Cerebral Cortex

DOI:10.1093/cercor/bhx191 Impact Factor 6,3

David S. Newburg, Ayse Ceren Tanritanir, Subrata Chakrabarti, *Lactodifucotetraose, a human milk oligosaccharide, attenuates platelet function and inflammatory cytokine release,* Journal of Thrombosis and Thrombolysis

DOI:10.1007/s11239-015-1331-2 Impact Factor 2,7

Danksagung

An erster Stelle möchte ich meinem Doktorvater, Herrn Professor Jochen B. Fiebach, danken. Durch seine Anregungen hat meine Dissertation den richtigen Schliff bekommen und eine gute Wendung genommen. Er hat mir mit viel Interesse und Hilfsbereitschaft zur Seite gestanden. Herzlichen Dank dafür. Ein weiterer herzlicher Dank gilt auch meinem Betreuer, Herrn Dr. Ahmed A. Khalil. Zu jeder Zeit hat er mich mit konstruktiven Ratschlägen unterstützt und hat mit seiner umsichtigen und hilfsbereiten Art ganz wesentlich zum Gelingen dieser Arbeit beigetragen. Vielen Dank lieber Ahmed, dass du bei jeglichen Fragen stets ein Ansprechpartner für mich warst und mich bei meiner Arbeit durchgehend gefordert hast.

Ein weiterer Dank gilt den CO-Autoren Frau Ulrike Grittner, ohne die ich an Statistik gescheitert wäre, und Frau Dr. Ivana Galinovic sowie Dr. Kerstin Villringer, die mich durch ihre hilfreichen Kommentare und Ideen in meiner Tätigkeit bestärkt haben.
Weiterhin möchte ich mich bei meinem Lebenspartner Heider Ridha bedanken. Ohne unsere magische Begegnung hätte ich meine große Liebe für Entdeckung und Lernen nicht weiter entwickelt.

Ein besonderer Dank gilt meinen Eltern, Frau Filiz Ateş und Herrn Dr. Ahmet Tanrıtanır, und meinem Bruder Ömer Tanrıtanır. Sie haben mich bei meiner Entscheidung, nach Deutschland zu ziehen, immer finanziell und emotional unterstützt und dafür immer großes Verständnis gezeigt. Sie haben mich ermutigt, ständig zu lernen, zu fragen und zu entdecken.

Abschließend möchte ich meiner Großmutter, Şenel Ateş, danken, der ich diese Arbeit widme. Ohne ihre häufigen aufmunternden Worte wäre diese Arbeit nicht zustande gekommen.

Ich wurde immer wieder von Familie, Kollegen und Freunden ermutigt, dranzubleiben und meine Promotion abzuschließen. Dafür bin ich allen sehr dankbar.